Meteorology-Aware Multi-Goal Path Planning for Large-Scale Inspection Missions with Solar-Powered Aircraft

Philipp Oettershagen*, Julian Förster†, Lukas Wirth†, Gregory Hitz‡ and Roland Siegwart§
Swiss Federal Institute of Technology (ETH Zurich), Leonhardstrasse 21, 8092 Zurich, Switzerland

Jacques Ambühl¶
Swiss Federal Office of Meteorology and Climatology, Operation Center 1, 8058 Zurich-Airport, Switzerland

Solar-powered aircraft promise significantly increased flight endurance over conventional aircraft. While this enables large-scale inspection missions, their fragility necessitates that adverse weather is avoided. This paper therefore presents MetPASS, the Meteorology-aware Trajectory Planning and Analysis Software for Solar-powered Unmanned Aerial Vehicles (UAVs). MetPASS is the literature's first path planning framework that considers all safety- and performance-relevant aspects of solar flight: It avoids terrain collisions and no-fly zones, integrates global weather data (sun radiation, wind, gusts, humidity, rain and thunderstorms) and features a comprehensive energetic model to avoid system risks such as low battery charge. MetPASS leverages Dynamic programming and an A*-search-algorithm with a custom cost function and heuristic to plan globally optimal point-to-point or multi-goal paths with coverage guarantees. A full software implementation is provided. The planning results are analyzed using missions of ETH Zurich's *AtlantikSolar* UAV: An 81-hour stationkeeping flight, a hypothetical 4000 km Atlantic crossing and two multi-glacier inspection missions above the Arctic Ocean. It is shown that integrating meteorological data is indispensable for reliable large-scale solar aircraft operations. For example, the nominal no-wind flight time of 106 h across the Atlantic is reduced to 52 h by selecting the correct launch date and flight path.

I. Introduction

A. Motivation

Solar-powered Unmanned Aerial Vehicles (UAVs) promise significantly increased flight endurance over conventional aircraft. This greatly benefits applications such as large-scale disaster relief, border patrol or aerial inspection in remote areas [1]. Research and development of solar UAVs is ongoing in both academia [2, 3] and industry [4, 5]. Since

*PhD student, Autonomous Systems Lab, Department of Mechanical and Process Engineering, philipp.oettershagen@mavt.ethz.ch
†Master student, Autonomous Systems Lab, Department of Mechanical and Process Engineering
‡Senior researcher, Autonomous Systems Lab, Department of Mechanical and Process Engineering, gregory.hitz@mavt.ethz.ch
§Professor, Autonomous Systems Lab, Department of Mechanical and Process Engineering, rsiegwart@ethz.ch
¶Retired ; Formerly research meteorologist, Department Analysis and Forecasting, ambuhl@icloud.com

2005, multiple solar aircraft have demonstrated multi-day continuous flight [6–8], with the world record being a 14-day continuous flight [9]. In our own work [10], we have previously shown an 81-hour continuous solar-powered flight with the *AtlantikSolar* UAV (Fig. 1) which set the current flight endurance world record for aircraft below 50 kg total mass.

However, all solar-powered aircraft require suitable weather conditions for long-endurance operations. Thunderstorms, rain and wind gusts are elementary threats to the aircraft's integrity. Moreover, clouds and strong winds can significantly reduce the solar power income or increase the required propulsion power such that landing is required. Solar aircraft, and more generally all aerial vehicles that are weather-sensitive either because they are flying slowly or are structurally fragile, therefore require careful pre-operational planning. Safe and efficient flight requires the consideration of terrain, the internal system state (e.g. battery state of charge), and major weather phenomena (thunderstorms, rain, winds and wind gusts, radiation and clouds). A model-based path planning framework allows to integrate these effects in a structured manner and is thereby able to generate globally optimal flight paths (Fig. 1).

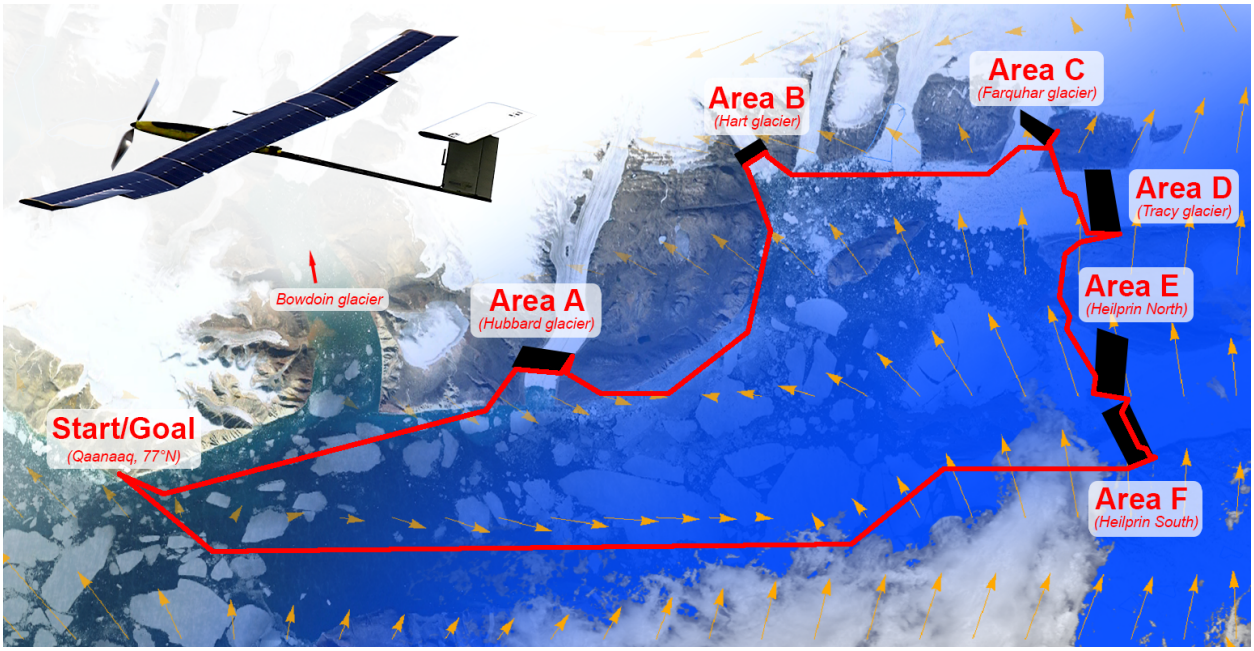

Fig. 1 Large-scale aerial sensing missions with solar aircraft such as *AtlantikSolar* (top left) require careful planning. MetPASS, the Meteorology-aware Trajectory Planning and Analysis Software for Solar-powered UAVs presented herein, plans optimal point-to-point and multi-goal routes that allow inspecting multiple areas of interest — for example Arctic glaciers — in one flight. These routes are safe and efficient given the consideration of terrain and meteorological risks such as wind, rain, thunderstorms and clouds.

B. State of the art

Literature on path planning for solar-powered aircraft is sparse. The individual elements (e.g. wind-dependence, sun-dependence) are only considered separately in relatively unrelated fields of research. On one hand, when focussing only on wind-aware planning, comprehensive research is available. Sridhar [11] presents optimal-control based path

planning in 2D winds to avoid creating condensation trails. Rubio [12] proposes evolutionary approaches and considers 3D wind fields in a large-scale Pacific crossing mission. A planner for oceanic search missions, which employs temperature and humidity data to predict icing conditions, is presented in subsequent work [13]. Chakrabarty presents an A*-based planner for soaring in realistic wind fields [14] and a sampling-based planner for paths through complex time-varying 3D wind fields [15]. All these contributions focus on either fuel-powered or non-solar gliding aircraft. On the other hand, research which incorporates solar models mostly neglects wind and thus solves a very simplified problem. For example, Klesh [16, 17] uses optimal control techniques to generate paths maximizing the UAV's final energy state in small-scale point-to-point and loitering problems, but assumes a constant sun position. Spangelo [18] investigates optimal climb and descent maneuvers during loitering. Hosseini [19] adds sun-position time dependence, but assumes perfect clear-sky conditions. Dai [20] avoids the clear-sky assumption by deriving an expected solar radiation income based on local precipitation and humidity forecasts. The path planning problem is then solved by a Bellman-Ford algorithm. Overall, there is no literature that covers all the system-related or meteorological aspects that affect solar aircraft. In addition, there is a clear lack of flight test based verification of planning approaches.

C. Contributions

This paper presents the Meteorology-aware Trajectory Planning and Analysis Software for Solar UAVs (MetPASS), the literature's first path planning framework that considers all major safety and performance relevant aspects (terrain, no-fly zones*, system state, meteorology) of solar-powered flight. It optimizes large-scale stationkeeping, point-to-point and multi-goal missions (Fig. 1) and focusses on real-world applications. The technical contributions of this paper are:

- an *optimization approach* that yields cost-optimal aircraft paths by combining an extended A*-algorithm for multi-goal order optimization, a Dynamic Programming (DP) based point-to-point planner and a local scan path planner that guarantees area coverage using a simple camera model.
- a *cost function* for safe and efficient solar-powered flight. It considers the terrain collision risk, system state (time since launch, battery state of charge, power consumption and generation) via a comprehensive energetic model, and up-to-date global weather data (thunderstorms, rain, humidity, 2D winds, gusts, sun radiation and clouds).
- a *full software implementation* with a GUI and computational speed optimizations (custom-designed heuristic, parallelization and caching). Mission feasibility analysis, pre-flight planning and in-flight replanning are supported.
- an extensive *flight-test based analysis* of the planning results using the 81-hour flight endurance record of *AtlantikSolar* [10], a hypothetical crossing of the Atlantic Ocean from Newfoundland to Portugal, and two multi-goal glacier inspection missions above the Arctic Ocean near Greenland.

This article is a *systems* paper. Its contributions are of practical rather than purely theoretical nature: It is the first article in the literature that carefully *identifies and selects* the most suitable *existing* planning methods (DP, extended

*Used for example to model zones with dense air traffic

A*) and *optimizes and integrates* them with solar-flight-specific components (custom system model, cost function, heuristics and ECMWF/COSMO weather model interface) to create a *practical* (fast yet sufficiently accurate) solar flight planner. The results thus do not focus on planning method performance comparisons (given that DP and A* are well explored performance-wise), but on, first, showing *that* and *how* reliable real-world solar flight planning can be performed and, second, demonstrating solar UAV potential in large-scale missions when guided by such a planner. The crucial challenge lies in accumulating the knowledge — and real world experience — in solar aircraft design, operations as well as meteorology and correctly and efficiently fusing them in a planner. This is obvious in the existing literature: While a plethora of theoretically-involved optimizers exists (Section I.B), these over-simplify the characteristics of solar flight and have thus not led to any meaningful large-scale solar flights. This paper seeks to be different.

This paper is organized as follows: Section II summarizes the DP-based point-to-point path planning (initially presented in [21]) and introduces the new A*-based multi-goal optimization approach with local scan path planning and terrain avoidance. Section III describes the software implementation. Section IV presents planning results and the flight test based analysis (both significant extensions of [21]). Section V provides concluding remarks.

II. Design

MetPASS (Fig. 2) plans safe and efficient large-scale aerial inspection missions for fixed-wing aircraft and solar-powered aircraft in particular. In the multi-goal mission case, a *multi-goal path planner* performs the *scan path optimization* within each area of interest. Using the scan paths, the *inter-goal path optimization* then determines the order to visit the areas of interest. The *point-to-point planner* optimizes the individual routes between areas of interest.

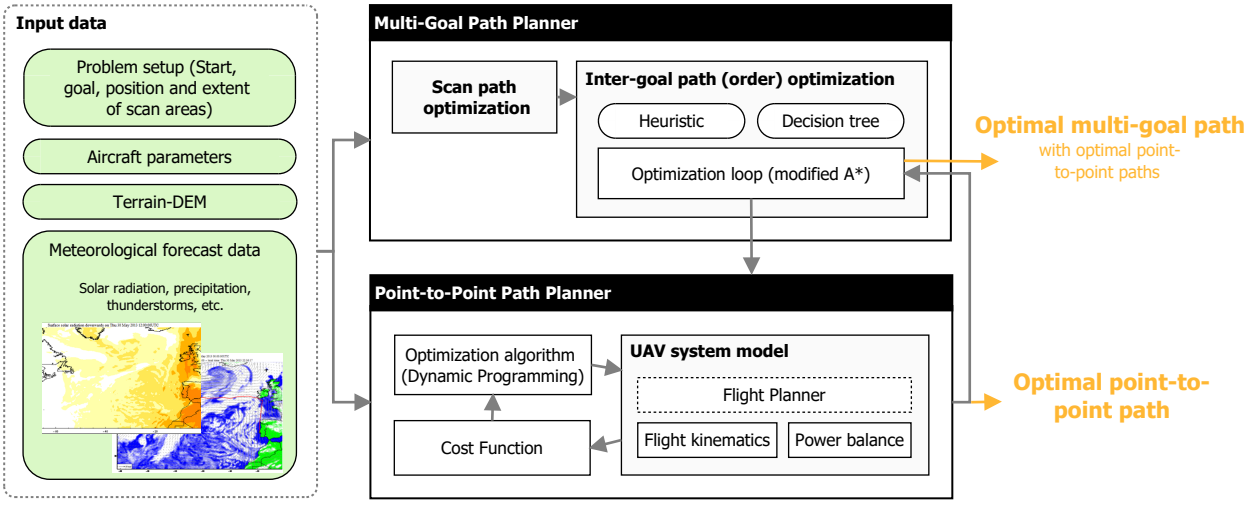

Fig. 2 MetPASS architecture.

A. Environment-Aware Point-to-Point Path Planning

The optimization problem solved by the MetPASS point-to-point planner (Fig. 2) is: Given fixed departure and arrival coordinates, find a path which minimizes the total cost as defined by a cost function while obeying user-specified no-fly zones (set e.g. based on Notice to Airmen or NOTAMs). The cost function includes terms for the proximity to terrain, the environmental conditions, and the system state. The departure time can be a fixed or free parameter.

1. Optimization Algorithm

The optimization is based on the well-known dynamic programming [22, 23] technique and extends Ambühl's [24] implementation with altitude optimization. The working principle is shown in Fig. 3: A three-dimensional grid between the departure and arrival points with, horizontally, i slices of j vertices and, vertically, k levels is generated. Starting from the departure node, the cost to each subsequent node is calculated. Then, starting from the nodes in slice three, the DP algorithm

$$d_{i,j,k} = \min_{n \in \mathrm{slice}_{i-1}} \left[d_{i-1,n} + \Delta_{i-1,n}^{i,j,k} \right] \tag{1}$$

finds the shortest total distance $d_{i,j,k}$ from the departure point to each grid node by minimizing the sum of a priori known distances $d_{i-1,n}$ and the additional distance $\Delta_{i-1,n}^{i,j,k}$. A decision tree of globally optimal sub routes is thus built up and finally reaches the arrival point. The optimal path is extracted by going back up the tree from the arrival point. In contrast to this simplified distance optimization, the real cost function depends on time-varying weather data and a comprehensive system model. Each path segment is thus simulated using numerical integration.

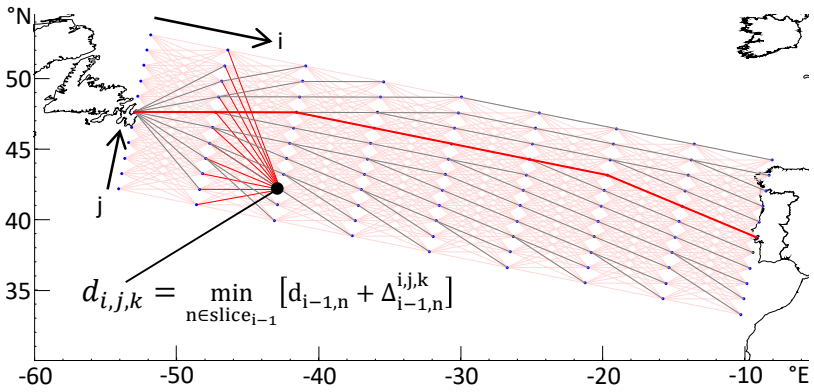

Fig. 3 Exemplary route optimization from start (Canada) to goal (Portugal) on a rectangular grid. The dynamic programming algorithm of Eq. (1) is applied to the grid points i,j in horizontal and k in vertical direction (not shown). The thick red line is the optimal path.

2. Cost Function

For solar-powered aircraft, an optimal path is not necessarily the shortest path, but the one with the highest probability of mission success and thus the lowest accumulated risk exposure. The cost function mathematically considers risk

through *cost terms* which can be grouped as follows:

- *Flight time*. This mainly becomes of importance if all other costs are small.
- *Environmental costs*: The environmental (or meteorological) costs indicate an environmental threat to the airplane. This includes strong wind, wind gusts, humidity, precipitation and thunderstorms.
- *System costs*: Includes State of Charge (SoC), power consumption and the radiation factor, which is the ratio between current and clear-sky solar radiation and thus indicates clouds. Flight states with low SoC, high power consumption or low radiation factor are avoided by flying at the power-optimal airspeed and evading clouded areas.
- *Distance to terrain*: Based on a Digital Elevation Model (DEM), this term helps to avoid terrain collisions while flying in cluttered terrain. The cost term has been extended with respect to our previous work [21].

The instantaneous flight time cost is simply the so called flight time cost factor, i.e. $\dot{C}_{\text{time}} = c_{\text{time}}$. All other costs $\dot{C}_k$ need to be normalized to allow for a consistent summation and weighting via

$$\dot{C}_k = H\big(\text{sgn}(\beta_k - \alpha_k) \cdot (x_k - \alpha_k)\big) \cdot \frac{\exp\left(\frac{x_k - \alpha_k}{\beta_k - \alpha_k} \epsilon_k\right) - 1}{\exp\left(\epsilon_k\right) - 1} \,, \tag{2}$$

where $sgn(...)$ is the signum function. As illustrated in Fig. 4, α_k and β_k define the lower threshold and the upper limit where the generated cost is bounded. Due to the Heaviside function $H(...)$ values x_k below the threshold generate no cost because they are not in a critical range. Values above the limit are considered too dangerous for the aircraft and thus cause a cancellation of the corresponding path. The exponent ϵ_k determines the cost function curvature. The accumulated overall cost for a path segment is finally calculated by summing up all 10 costs to a total cost and integrating it over the flight time:

$$C = \int_{t_1}^{t_2} \sum_{k=1}^{10} \dot{C}_k \, dt \,. \tag{3}$$

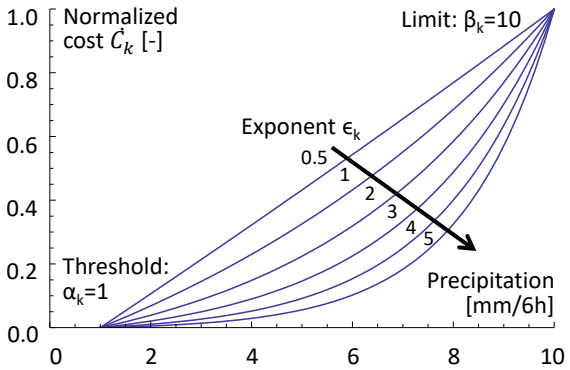

Fig. 4 Exemplary cost function (precipitation cost) and the parameters available to adjust its sensitivity.

Table 1 Forecast parameters received from the ECMWF and COSMO models.

Parameter	Unit	Description	Type
Temperature	°C		3D
Relative humidity	%		3D
Horizontal wind	m/s	Lateral and longitudinal winds	3D
Wind gusts	m/s	Max. wind gust over last time step	2D
Total precipitation	mm	Accumulated over last time step	2D
Convective available potential energy (CAPE)	J/kg	Causes updrafts and thunderstorms	2D
Total solar radiation (direct + diffuse)	J/m²	Accumulated over last time step	2D
Direct solar radiation	J/m²	Accumulated over last time step	2D

3. Meteorological Forecast Data

The weather data used for solar flight modeling is given in Table 1. Both historical data for mission feasibility analysis and forecast data to pre-plan or re-plan missions on site are supported. The European Centre for Medium-Range Weather Forecasts (ECMWF) global deterministic IFS-HRES model (horizontal resolution of 0.125 °) or the European COSMO model (resolution up to 2 km) are used at time steps between 1–6 hours and altitude levels between 0 m and 1600 m above mean sea level (Table 2). The data is linearly interpolated in time and in all three spatial dimensions. Correctly integrating the extensive weather model data is a significant challenge, with details given in [25].

4. System Model

The system model (Fig. 5) calculates the states for the cost function in a deterministic manner. Given the mission time scales of hours or days, aircraft dynamics are neglected. Instead, the `Aircraft Kinematic Model` simply updates the position using the airspeed and the calculated wind angle and ground speed. The airspeed is determined by the `Flight Planner`, which represents the UAV decision logic: The airspeed may be increased, first, in headwind to maintain a certain ground speed or, second, if excess solar power is available, the battery is fully charged and the aircraft is already at the maximum admissible altitude. The flight planner can also increase the altitude once SoC = 100 % to store solar energy into potential energy or to use favorable winds at higher altitude. The power balance is estimated by the `Aircraft System Model`. The direct and diffuse solar radiation are considered separately: The incidence angle φ_k is calculated using solar radiation models [25–27] and the geometry of the aircraft and solar modules k. For the diffuse radiation the incidence angle is neglected. With the solar module areas A_k, the temperature dependent solar module efficiency η_{sm} and the Maximum Power Point Tracker efficiency η_{MPPT}, the incoming power is

$$P_{\mathrm{solar},k} = \left(I_{\mathrm{diff}} + I_{\mathrm{direct}} \cdot \cos(\varphi_k)\right) \cdot A_k \cdot \eta_{\mathrm{sm}} \cdot \eta_{\mathrm{MPPT}} \tag{4}$$

$$P_{\mathrm{solar}} = \textstyle\sum_k P_{\mathrm{solar},k} \tag{5}$$

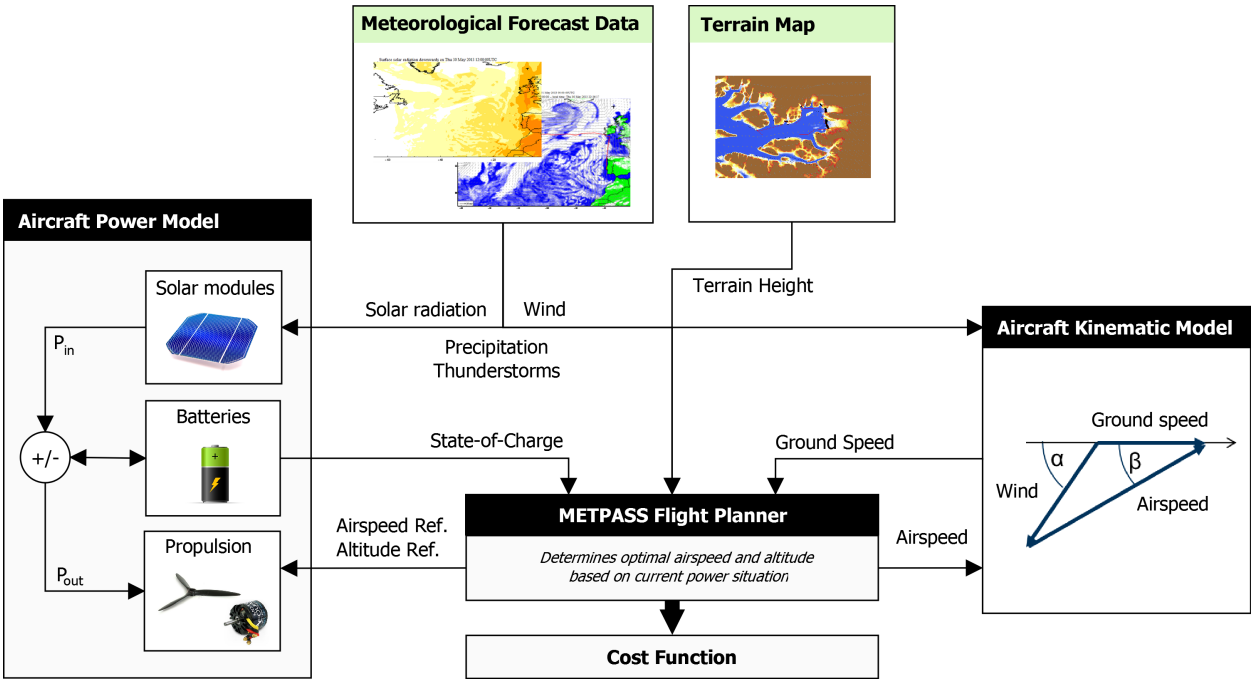

Fig. 5 The MetPASS system model and the interactions with the Flight Planner module.

The overall level-flight power consumption depends on the airspeed v_{air} and the altitude and thus air density ρ:

$$P_{\text{level}}(\rho, v_{\text{air}}) = \frac{P_{\text{prop}}(\rho, v_{\text{air}})}{\eta_{\text{prop}}(\rho, v_{\text{air}})} + P_{\text{av}} + P_{\text{pld}} \,, \tag{6}$$

where $P_{\text{prop}}/\eta_{\text{prop}}$ determines the required electrical propulsion power, and P_{av} and P_{pld} are avionics and payload power respectively. In our case, the dependence of P_{level} on the airspeed v_{air} is modeled through

$$P_{\text{level}}(\rho_0, v_{\text{air}}) = C_2 \cdot v_{\text{air}}^2 + C_1 \cdot v_{\text{air}} + C_0 \tag{7}$$

which is identified directly from *AtlantikSolar* power measurement test flights performed at constant altitude and thus air density ρ_0. The scaling to different altitudes or air densities is done according to [28] using

$$P_{\text{level}}(\rho, v_{\text{air}}) = \sqrt{\frac{\rho_0}{\rho}} \cdot \left[C_2 v_{\text{air}}^2 \frac{\rho}{\rho_0} + C_1 v_{\text{air}} \sqrt{\frac{\rho}{\rho_0}} + C_0 \right] \,. \tag{8}$$

With the airplane mass m_{tot}, climb rate $\dot{h}$, and climb efficiency η_{climb}, the total flight power P_{flight} is

$$P_{\text{flight}}(\rho, v_{\text{air}}) = P_{\text{level}}(\rho, v_{\text{air}}) + \frac{m_{\text{tot}} g \dot{h}}{\eta_{\text{climb}}} \,. \tag{9}$$

Defining the total battery energy E_{bat} and the battery efficiency η_{charge}, the SoC is updated by

$$\dot{\text{SoC}} = \frac{P_{\text{solar}} - P_{\text{flight}}}{E_{\text{bat}}} \eta_{\text{charge}} \ . \tag{10}$$

Note that $0 < \text{SoC} < 1$ and a charge rate limit for large SoC's is enforced.

B. Environment-Aware Multi-Goal Path Planning

Given fixed start and goal coordinates S and G and a set of convex polygonal areas of interest (called *nodes* $\mathcal{N}$), the multi-goal path planning finds the optimal node-order and thus global path. Two sub-functions, i.e. the *scan path optimization* which calculates the scan path inside each area of interest and the *inter goal path planner* which determines the order of and the trajectories in between the areas of interest, are visualized in Fig. 6.

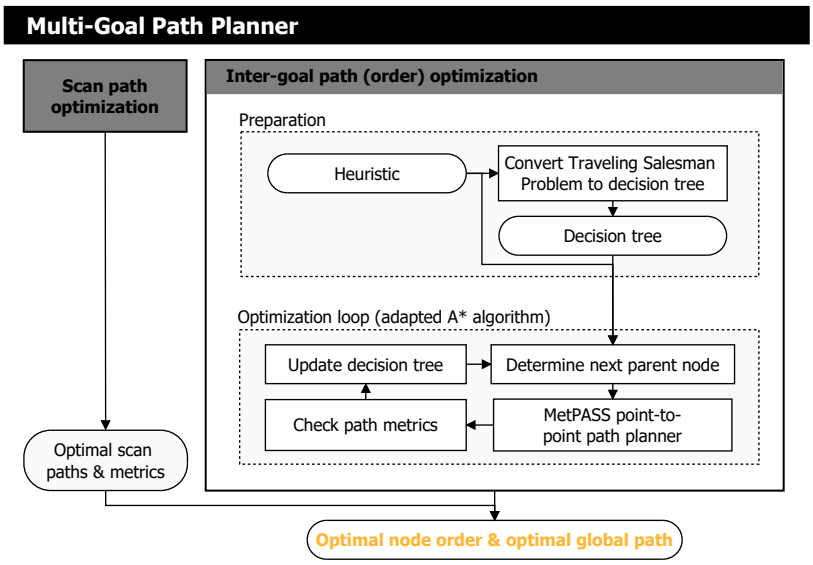

Fig. 6 The multi-goal path planning module, which is part of the overall architecture shown in Fig. 2.

1. Scan Path Optimization

The scan path optimization is carried out independently for each area of interest. The problem can be stated as: Given a) the convex polygonal area of interest, b) scan parameters such as altitude, airspeed, camera field of view and image overlap, and c) weather data, find a scan path that guarantees coverage of the area of interest at minimum cost. For simplicity, lawn-mower scan patterns (Fig. 7) are employed and optimized for the course angle. For constant wind and lawn-mower patterns with equal outward/backward-distance, a course perpendicular to the wind results in minimum flight time. However, in our case the wind varies in space, the polygon can be of arbitrary convex shape, and we aim for minimum cost instead of minimum flight time such that the solar power income over all course angles needs to be considered. Thus, the course angle has to be optimized via simulating scan paths over a range of course angles using the

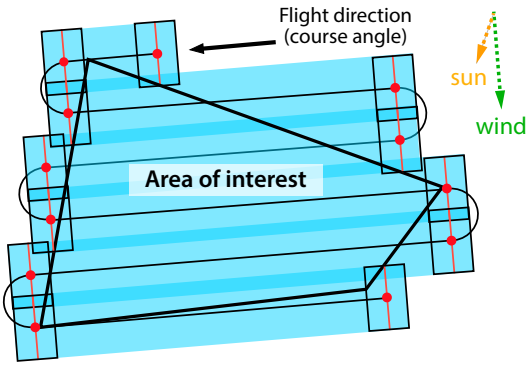

Fig. 7 A lawn-mower scan path in an area of interest. The black arrow is the flight direction (course) and the rectangles are selected camera images. The optimization considers environmental factors such as wind and sun.

system model of Section II.A.4. The optimal polygon corner to start from is found in the same process. The final results are the optimized scan path (Fig. 7) and the path length, flight time, cost, and state of charge change ΔSoC.

2. Inter-Goal Path Optimization

The inter-goal path optimization finds the optimal node order. For minimum distance, the trivial circular path in Fig. 1 is a good solution to this well known Traveling Salesman Problem (TSP) [29]. However, our optimization objective is minimum cost, our problem is time-dependent because of weather changes and it is also asymmetric because, for example in wind, flying from node A to B can cause a different cost than flying from B to A. We therefore have to solve a Time Dependent Asymmetric Traveling Salesman Problem (TDATSP). Both the TSP and TDATSP are computationally expensive NP-hard problems. The brute-force approach to solving the TSP is of order $O(N!)$, where N is the number of nodes excluding the start/goal node. For our applications we mostly have $N < 10$, however, each point-to-point optimization solves a dynamic programming problem that typically consumes 3–600 s (Table 4). The algorithms solving the TDATSP should thus decrease the number of required edge cost calculations.

Solving the time-dependent asymmetric traveling salesman problem Dynamic programming approaches for the TSP were introduced by Bellman [30]. More recently, Malandraki introduced an optimal DP approach [31] and a faster restricted DP method [32] for the TDATSP. However, the former requires the computation of all edge costs, while the latter does not guarantee optimality. Similarly, the Simulated Annealing approach by Schneider [33] and the genetic algorithms by Testa [34] do not guarantee optimality. However, efficient label correcting methods can be applied if the TDATSP is converted into a Time-Dependent Shortest-Path Problem (TDSPP) [35]. This approach is chosen for this paper. The resulting tree is shown in Fig. 8. While the original TSP contains the $N = 3$ nodes $\mathcal{N} = \{1, 2, 3\}$ excluding the start/goal nodes, the SPP graph contains the $V = 21$ vertices $\mathcal{V} = \{S1, S2, S3, S12, \ldots, S312G, S321G\}$ excluding the start vertex S but including those vertices[†] that finish with the goal node G. The root of the SPP graph represents

[†]The indices $n, m \in \mathcal{N}$ always refer to nodes while the indices $v, w \in \mathcal{V}$ always refer to vertices.

our start node S, and every branch is a valid (though not necessarily optimal or even feasible) solution path that covers all areas of interest and ends at the start node (called goal G for clarity) again. The cost for traversing an edge from vertex v to a child vertex w in the new graph is equal to the cost from the node n represented by the last digit in the parent label to the node m represented by the last digit in the child label. These costs are time dependent. A modified version of the A*-algorithm by Hart et al. [36] is selected to solve the TDSPP. With a properly designed heuristic, A* significantly reduces the required edge cost calculations while still providing optimality guarantees.

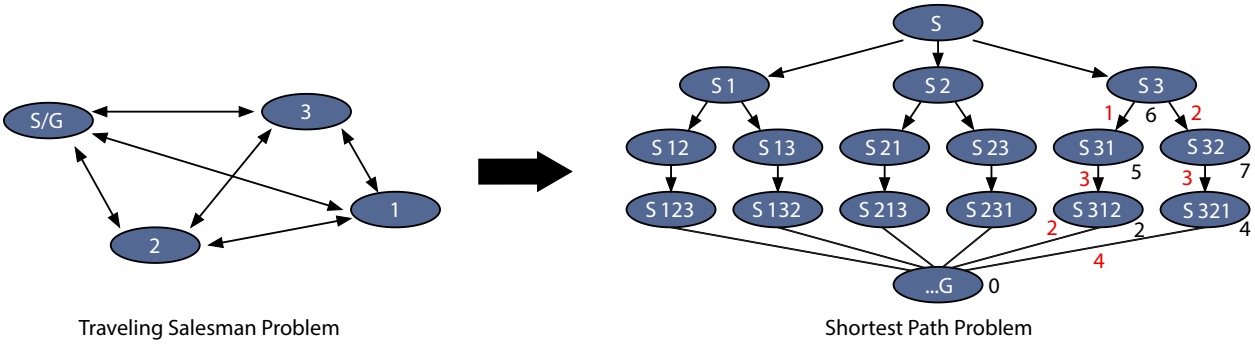

Fig. 8 Traveling salesman problem and the equivalent shortest-path problem that label correcting methods can be applied to. The SPP graph contains exemplary point-to-point (red) and cost-to-go (black) heuristics.

Heuristic calculation For every vertex $v \in \mathcal{V}$ in the SPP graph of Fig. 8, the heuristic h_v estimates the cost to fly to the goal G via all yet unvisited nodes. The heuristic has to be a lower bound on the path cost to avoid discarding optimal paths and to thus retain the optimality guarantee of A* [36]. However, the closer it is to the optimal path cost the larger the reduction in edge cost evaluations will be. The heuristic is calculated in two steps:

- First, a lower-bound cost estimate h_{nm} for a path from TSP node n to m is computed[‡]. As for the edge cost calculation we use Eq. (3), however, for the heuristic we assume a) a straight line (or orthodrome) path, b) start with full batteries and c) optimal weather conditions (e.g. tail wind, low cloud cover), which are searched over all grid points of the point-to-point mesh (Fig. 3) and all times within a user-specified time horizon.
- Second, the cost-to-go heuristic h_v is calculated for each vertex $v \in \mathcal{V}$ by summing up the point-to-point heuristics h_{nm} from the SPP graph's lowest level vertices (where $h_v = 0$) inside each tree to vertex v. If multiple paths are possible (e.g. vertex $S1 \rightarrow S12$ and $S1 \rightarrow S13$ in Fig. 8) then the lower-cost heuristic is chosen for the sum.

Optimization loop with an extended A*-algorithm The A*-algorithm in Alg. 1 uses the following notation: The current lowest cost to go from S to vertex $v \in \mathcal{V}$ is g_v and the cost to go from vertex v to vertex w is c_{vw}, where w is a successor of v and p_v is the parent of v on the shortest path from S to v found so far. The labels are designated as l. In contrast to the algorithm by Hart [36], the implementation in MetPASS is extended to consider

[‡] h_{nm} can be calculated between the nodes $\mathcal{N}$ of the TSP graph instead of the vertices $\mathcal{V}$ of the SPP graph because the point-to-point heuristic is time-independent.

- *The time dependence* of the edge costs due to weather changes. Each vertex v is assigned a departure time t_v.
- *The SoC dependence*. Each vertex v is assigned a departure state of charge SoC_v. The inter-vertex edge costs c_{vw} already include both the SoC and time dependency of the inter-node costs c_{nm}, i.e. $c_{vw} = c_{nm}(t_v, \mathrm{SoC}_v)$.
- *The scan path metrics*, i.e. the time and state of charge changes T_w and $\Delta\mathrm{SoC}_w$ at a certain SPP-vertex to inspect the related area of interest. Both T_w and $\Delta\mathrm{SoC}_w$ are assumed time-independent, i.e. can be replaced with the T_m and $\Delta\mathrm{SoC}_m$ of the corresponding node. The scan costs are thus the same for every SPP branch and don't need to be considered in the optimization. This speeds up planning significantly. However, if the ratio between the scan path time and the inter-goal path time exceeds a certain value, then the global path looses its optimality properties.

Under the assumption that the areas of interest are small compared to the total path length, this adapted A*-algorithm is still guaranteed to find the optimal multi-goal path: First, the principle of optimality [37] in the direction of execution (forward in our case) holds because our TDSPP graph is an *arborescence* (a special case of a *polytree*) and there is thus only a single path from S to any other vertex. Second, many comparable A*-extensions for time-dependent SPPs [38] require satisfying the first-in-first-out (FIFO) property $t_1 \leq t_2 \implies t_1 + t_{vw}(t_1) \leq t_2 + t_{vw}(t_2)$, which is automatically fulfilled in our case because our graph is a polytree and waiting at nodes is not allowed.

Algorithm 1 Extended A* to find the best path between start S and goal G. The cost c_{vw} and travel time t_{vw} incorporate the (t_v,SoC_v)-dependency. T_w and $\Delta\mathrm{SoC}_w$ are internally replaced with the time-independent T_m and $\Delta\mathrm{SoC}_m$.

$g_S, t_S \leftarrow 0$
$l_S \leftarrow$ "open"
$\mathrm{SoC}_S \leftarrow$ initial SoC specified by user
$g_k \leftarrow \infty \quad \forall k \in \mathcal{V}$
$l_k \leftarrow$ "unlabeled" $\quad \forall k \in \mathcal{V}$
$v \leftarrow S$
while $G \notin v$
do
- **for each** $w \in$ children(v)
  - **do**
    - **if** $g_v + c_{vw} < g_w$ **and** $g_v + c_{vw} + h_w < g_G$
      - **then**
        - $g_w \leftarrow g_v + c_{vw}$
        - $l_w \leftarrow$ "open"
        - $t_w \leftarrow t_v + t_{vw} + T_w$
        - $\mathrm{SoC}_w \leftarrow \mathrm{SoC}_v + \Delta\mathrm{SoC}_{vw} + \Delta\mathrm{SoC}_w$
        - $p_w \leftarrow v$
- $l_v \leftarrow$ "closed"
- $v \leftarrow$ "open" node with smallest value $g_k + h_k$

III. Implementation, Verification and Preliminary Results

A. Implementation

MetPASS is a Mathematica-based large-scale environment-aware mission planner for solar and standard battery-powered aircraft. MetPASS supports, first, mission feasibility analysis using historical weather data, second, finding

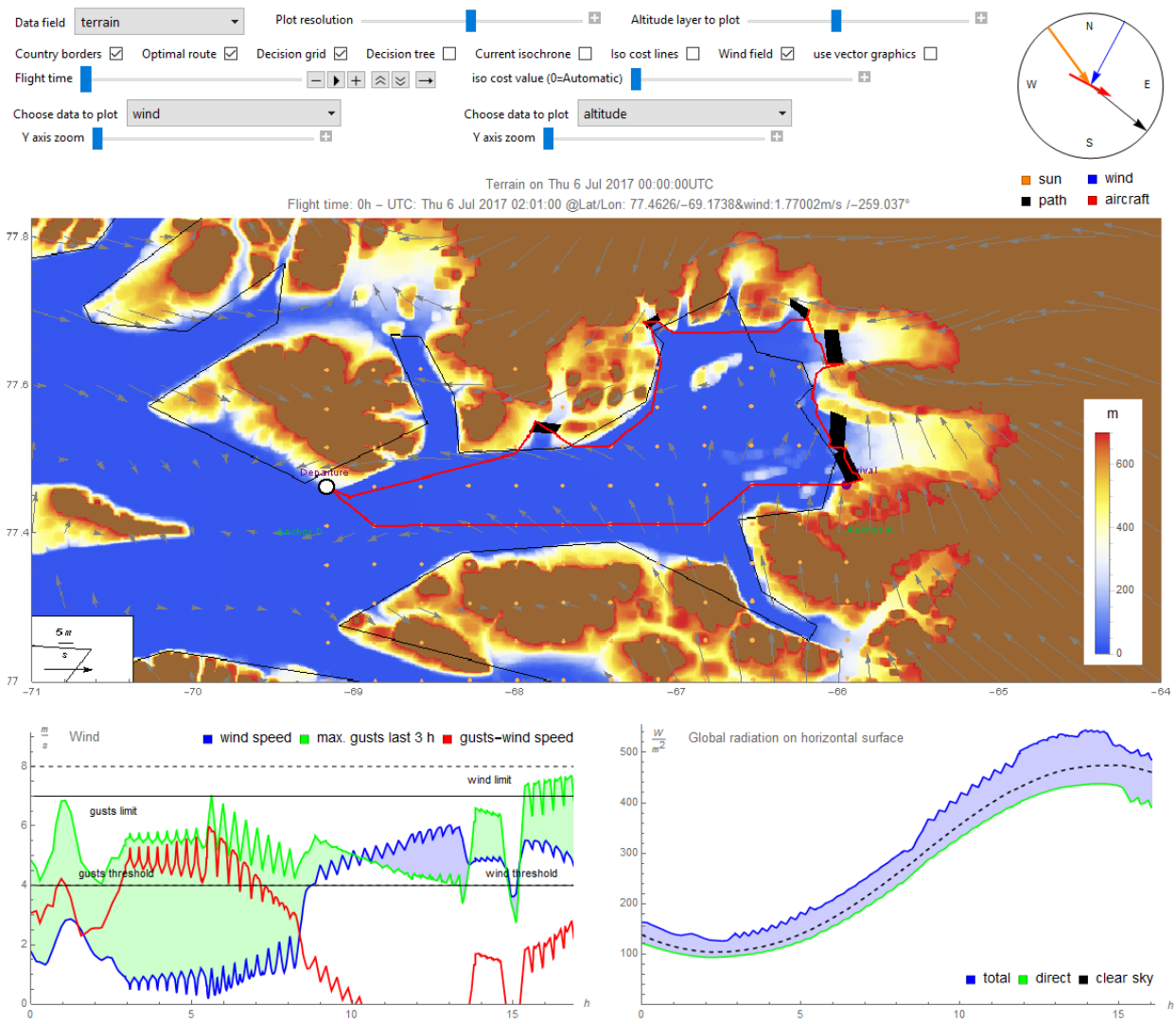

Fig. 9 MetPASS Graphical User Interface. Top left: Visualization controls. Top right: Sun, wind and path angle indicator. Center: Main visualization with areas of interest (black), proposed path (red), aircraft position (white dot), a terrain altitude map (color bar) and wind vector overlay (grey). Bottom: Wind speeds/gusts and solar radiation at the aircraft position over the full flight. MetPASS is implemented in *Wolfram Mathematica*.

the optimal launch time and pre-planning the mission on-site using weather forecast data, and third, re-optimizing the waypoints in flight once updated weather forecasts are available (see Section IV.B). During these processes, the MetPASS Graphical User Interface (Fig. 9) visualizes the flight path, terrain, environmental risks and system state to give the operator the means to assess whether a usually fragile and expensive solar aircraft can complete the mission. To allow fast on-site mission planning, MetPASS caches results (primarily heuristics and pre-planned scanned paths), leverages compiled C-code instead of much slower Mathematica-code, and supports parallel computation with up to $j \cdot k$ cores (j vertices, k altitude levels, see Fig. 3). To save edge cost evaluations, edge cost discretization over time and state of charge is also integrated, but was found [39] to only yield negligible performance improvements.

B. Validation and Preliminary Results

To independently verify the planner's system model and its optimization with respect to individual cost components, *unit tests* using the setup of Fig. 3 and only a subset of costs and weather parameters are performed. In the first unit test (Fig. 10), flight time is the only active cost. All weather parameters are set to default values (no wind and clear-sky solar radiation). The system model produces the expected results and the dynamic programming algorithm finds the time-optimal path (an orthodrome projected onto the grid). The flight planner increases the airspeed once SoC = 100 % and excess solar power is available. The flight time under this zero-wind condition is 106 h, the distance is 3650 km. In the second unit test (Fig. 11), the flight time is still the only cost, but time-varying ECMWF wind data is now considered. The 3D path optimization can be observed: The planner optimizes the altitude to exploit favorable winds at high altitude such that, overall, $v_{\text{gnd}} > v_{\text{air}}$. The flight time reduces from 106 h without wind to only 53 h. The third unit test (Fig. 12) combines only solar radiation, power consumption and flight time costs. The weather parameters are only direct and total solar radiation. The optimal path follows highly radiated areas during the day and the time-optimal path at night. The altitude changes prove that the power and flight time cost interaction works: The lowest altitude is chosen to minimize the power consumption, while the top altitude is only chosen to store potential energy or to increase the airspeed at a given power consumption once $SoC = 100\,\%$ and excess solar power is available. After unit testing, the cost parameters were refined to balance the influence of individual costs. Details on this process and the MetPASS validation are presented by Wirth [21, 25]. Table 2 contains the final parameters.

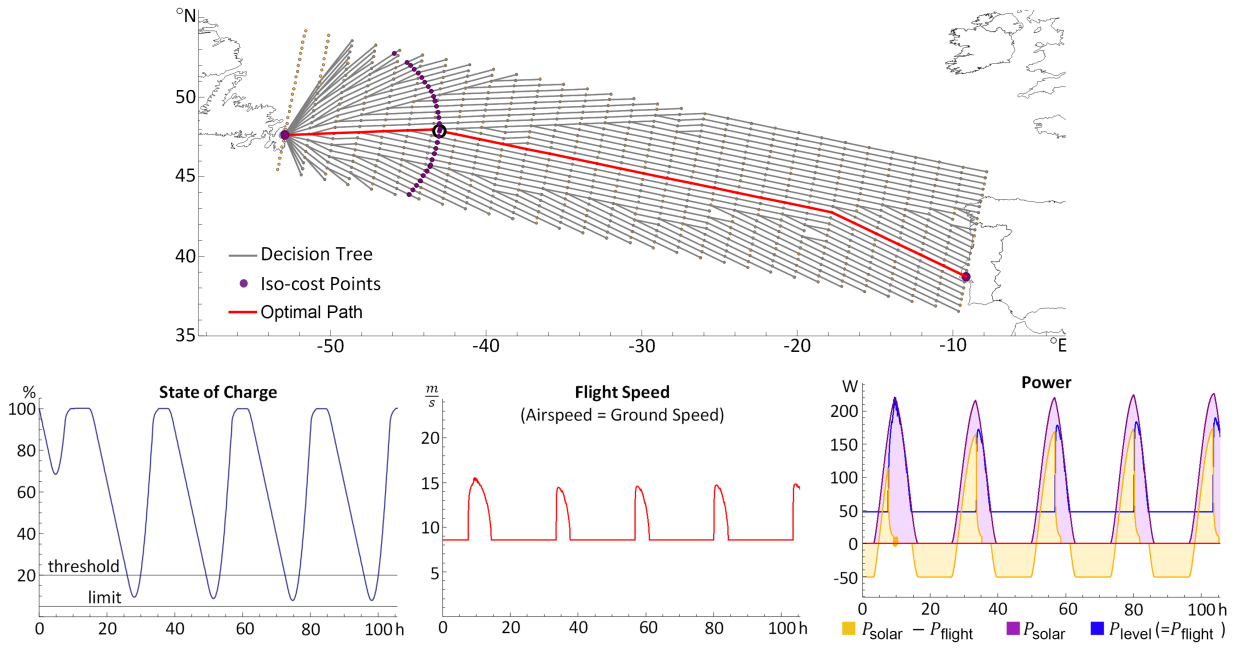

Fig. 10 First unit test: 2D, i.e. no altitude changes allowed, only time costs, default weather parameters. The iso-cost points form a circle around the start point. SoC and power income fluctuate with the day/night cycle. The flight planner increases the airspeed when SoC = 100 % and excess solar power is available.

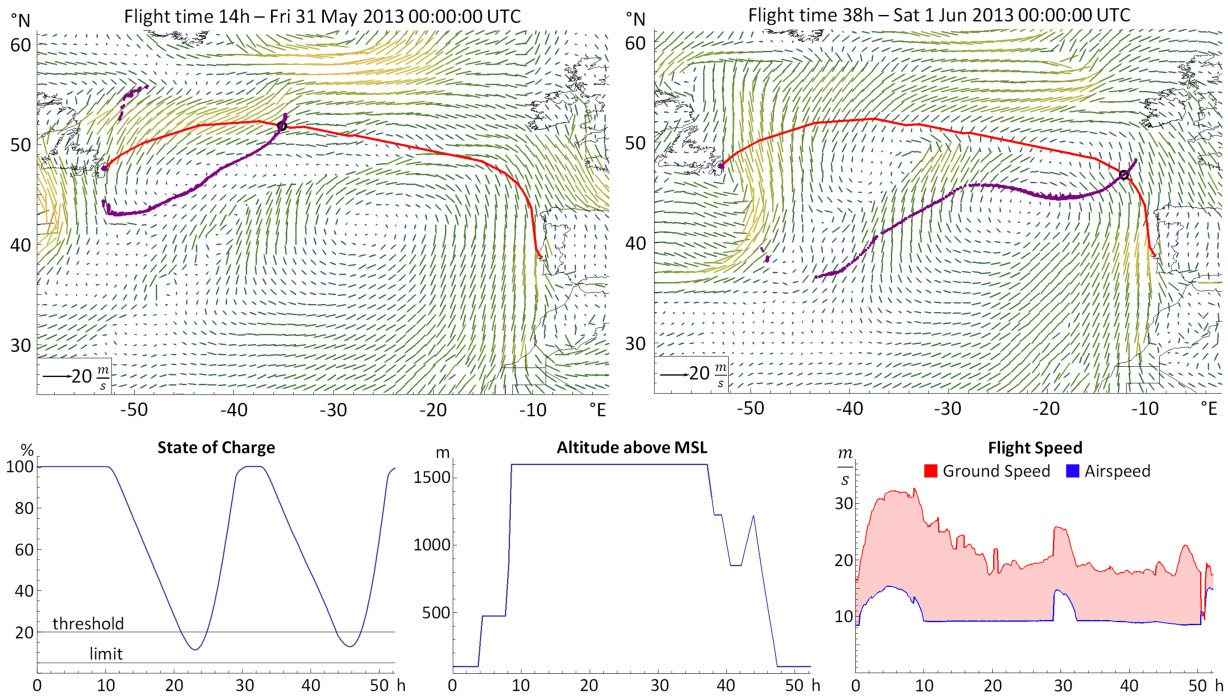

Fig. 11 Second unit test: 3D, i.e. altitude changes allowed, only time costs, wind conditions taken into account. The flight time is minimized by exploiting winds (including those at higher altitude) such that $v_{\mathrm{gnd}} > v_{\mathrm{air}}$. The flight time reduces from 106 h without wind to only 53 h.

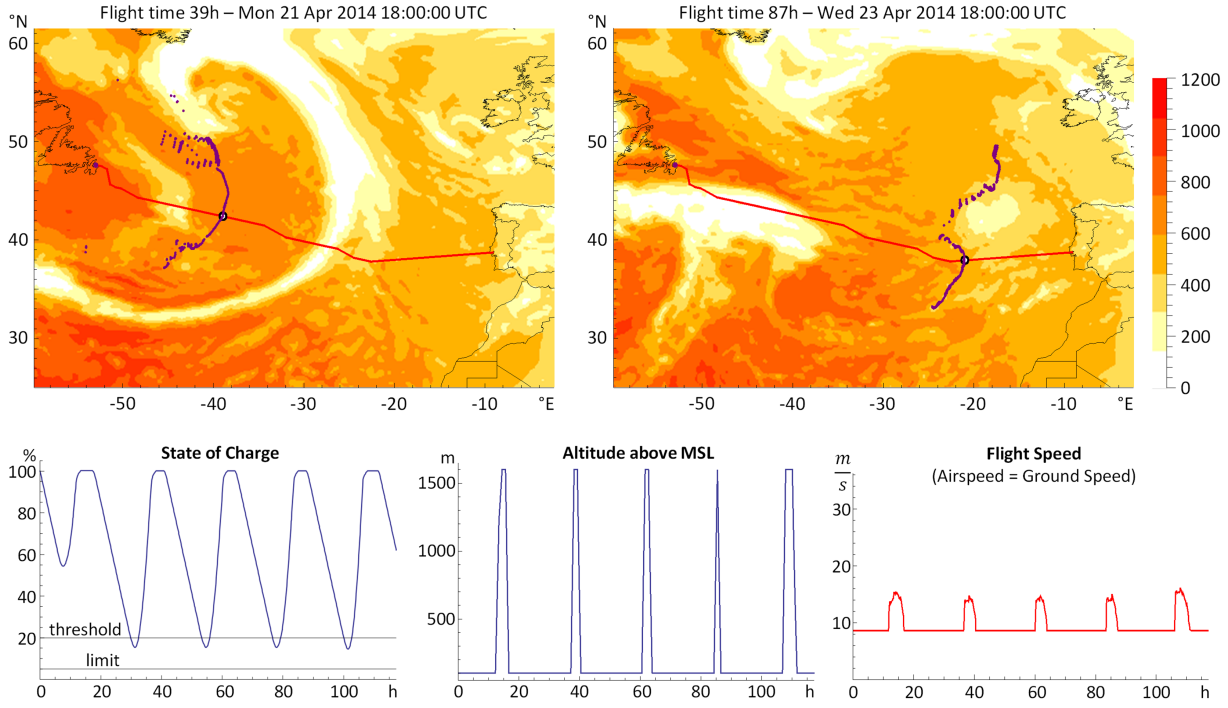

Fig. 12 Third unit test: The costs are solar radiation, power consumption and flight time. Only the radiation weather parameter is applied. Both altitude and airspeed are increased when $SoC = 100\,\%$ and excess solar power is available. The iso-cost points illustrate the influence of the radiation.

IV. Results

MetPASS was used to plan a demanding set of missions (Table 2) for ETH Zurich's *AtlantikSolar* UAV: First, the 81.5-hour stationkeeping mission [10] that set a flight endurance world record for aircraft below 50 kg is used to verify the MetPASS system model. Second, a hypothetical Atlantic crossing is presented. Third, two large-scale multi-goal glacier monitoring missions above the Arctic Ocean, attempted by *AtlantikSolar* in summer 2017, are discussed.

A. Loitering Mission: An 81-Hour Solar-Powered Flight

As described in our previous work [10] and a video[§], *AtlantikSolar* performed its 81.5-hour stationkeeping flight to demonstrate multi-day solar-powered flight with sufficient energetic margins for later telecommunications relay or aerial observation missions [40]. Clearly, such long-endurance missions require careful planning: While the trajectory is fixed, the launch date needs to be optimized and the mission feasibility under the given environmental conditions needs to be assessed. Using the weather *forecast* from before the flight, MetPASS indicated a 4-day weather window, and launch was thus performed on June 14th 2015 at 9:32 local time (8.00 solar time) at Rafz, Switzerland. While the weather forecasts were accurate for the first three days, they did not predict the thunderstorms and severe winds on the last day. To analyze the system models of Section II using correct weather data, Fig. 13 thus shows flight data and the MetPASS output based on *historical* weather data (i.e. a-posteriori COSMO-2 data with 2 km spatial and 1 h time resolution).

Given the clear-sky conditions MetPASS predicts a solar power income $P_{\text{solar}}^{\text{model}}$ close to the theoretical maximum of the full solar power model $P_{\text{solar}}^{\text{model}}$[FM] [41]. The lower power income on the last day due to clouds is captured correctly. The measured P_{solar} also closely follows the MetPASS predictions. It only deviates when SoC $\approx 100\,\%$ because P_{solar} is throttled down as per design to protect the batteries. The solar power therefore only covers the fluctuating propulsion demands. The power to sustain flight during the night is $P_{\text{bat}} = 41.6\,\text{W}$ whereas MetPASS estimates $P_{\text{bat}}^{\text{model}} = 42.4\,\text{W}$ using the measured power-curve fitted to Eq. (8). The predicted and measured minimum SoCs averaged over all three nights are 39 % and 40 % respectively. Notable deviations are only caused by unexpected evening thermals that cause altitude fluctuations and a decrease in P_{bat} during the first and third night. Overall, the MetPASS system model is very accurate. Of course, this is partially due to the irradiation conditions being close to the theoretical optimum.

The wind and airspeed plots show more variety: Strong winds are measured and modeled for the first day. In accordance with the ground operators, at $t = 15.4\,\text{h}$ solar time MetPASS suggests to increase the airspeed to assure $v_{\text{gnd}} > 0$. The winds decrease for the following nights, but reach up to 11.4 m/s (model) and 16 m/s (measurement) during the last flight hours. Both MetPASS and the operators increase the airspeed[¶] to assure $v_{\text{air}} \geq v_{\text{wind}}$. This shows how important MetPASS' automatic airspeed control functionality is to avoid vehicle drift-off. In addition, as indicated by the convective available potential energy (CAPE), thunderstorm clouds develop and the wind and thunderstorm costs

[§] https://www.youtube.com/watch?v=8m4_NpTQn0E

[¶] In contrast to MetPASS, the operators also increase the UAV altitude. This is one reason why the UAV measures higher wind speeds.

Table 2 Overview over the missions planned using MetPASS. The airplane parameters differ because three UAV versions (AS-1, AS-2 and AS-3) are used: η_{sm} and the battery energy density e_{bat} improve over time (but e_{bat} was decreased for the Arctic because of the low temperatures), and P_{flight} only increases because payload (e.g. cameras, satellite communication) was added. The cost parameters also vary: For example, the Atlantic mission (which was planned first, i.e. in 2014) had higher wind thresholds than the other two missions because constant winds were not considered as dangerous over the open ocean, much lower SoC limits because the AS-1 UAV performance was lower, and a lower time cost factor to put more emphasis on being safe rather than fast. In the Arctic missions, (A) represents Bowdoin and (B) represents the six-glacier mission.

Mission	**81h-flight** (Sec. IV.A)			**Atlantic** (Sec. IV.B)			**Arctic** (Sec. IV.C.1/IV.C.2)		
Path, grid and simulation parameters									
Mission type	Loitering			Point-to-point			Multi-goal		
Grid points (LxWxH)	1x1x1			40x113x5			A:30x25x1, B:12x9x1		
Altitude range (MSL)	600 m			100–1600 m			800 m		
Simulation time step	600 s			600 s			600 s		
Meteorological parameters									
Data type	Forecasts			Historical			Forecasts		
Model type	COSMO-2			ECMWF HRES			ECMWF HRES		
Long. resolution	2 km			0.125°			0.2°		
Lat. resolution	2 km			0.125°			0.1°		
Time resolution	1 h			6 h			3 h		
Airplane parameters									
Aircraft (Year)	AS-2 (2015)			AS-1 (2014)			AS-3 (2017)		
m_{tot}	6.9 kg			7.0 kg			7.4 kg		
m_{bat}	2.92 kg			2.92 kg			2.92 kg		
e_{bat}	240 Wh/kg			230 Wh/kg			222 Wh/kg		
η_{sm}	23.7 %			20.0 %			23.7 %		
$P_{\mathrm{flight}}(v_{\mathrm{air}}^{\mathrm{opt}})$	42 W			47 W			57 W		
Cost parameters									
	α	β	ϵ	α	β	ϵ	α	β	ϵ
State of charge	0.4	0.2	3	0.2	0.05	3	0.4	0.2	3
Radiation factor	0.8	0.05	3	0.8	0.05	3	0.8	0.05	3
Exc. power cons.	0	200	1	0	200	1	0	200	1
CAPE	100	2000	3	100	1000	3	100	1000	3
Wind	6	12	3	20	40	3	6	12	3
Wind gusts	9	15	3	5	20	3	9	15	3
Precipitation	0.1	10	3	1	10	3	0.1	10	3
Humidity	80	100	5	80	100	5	80	100	5
Altitude AGL	-	-	-	-	-	-	600	170	5
Time cost factor	0.05			0.01			0.05		

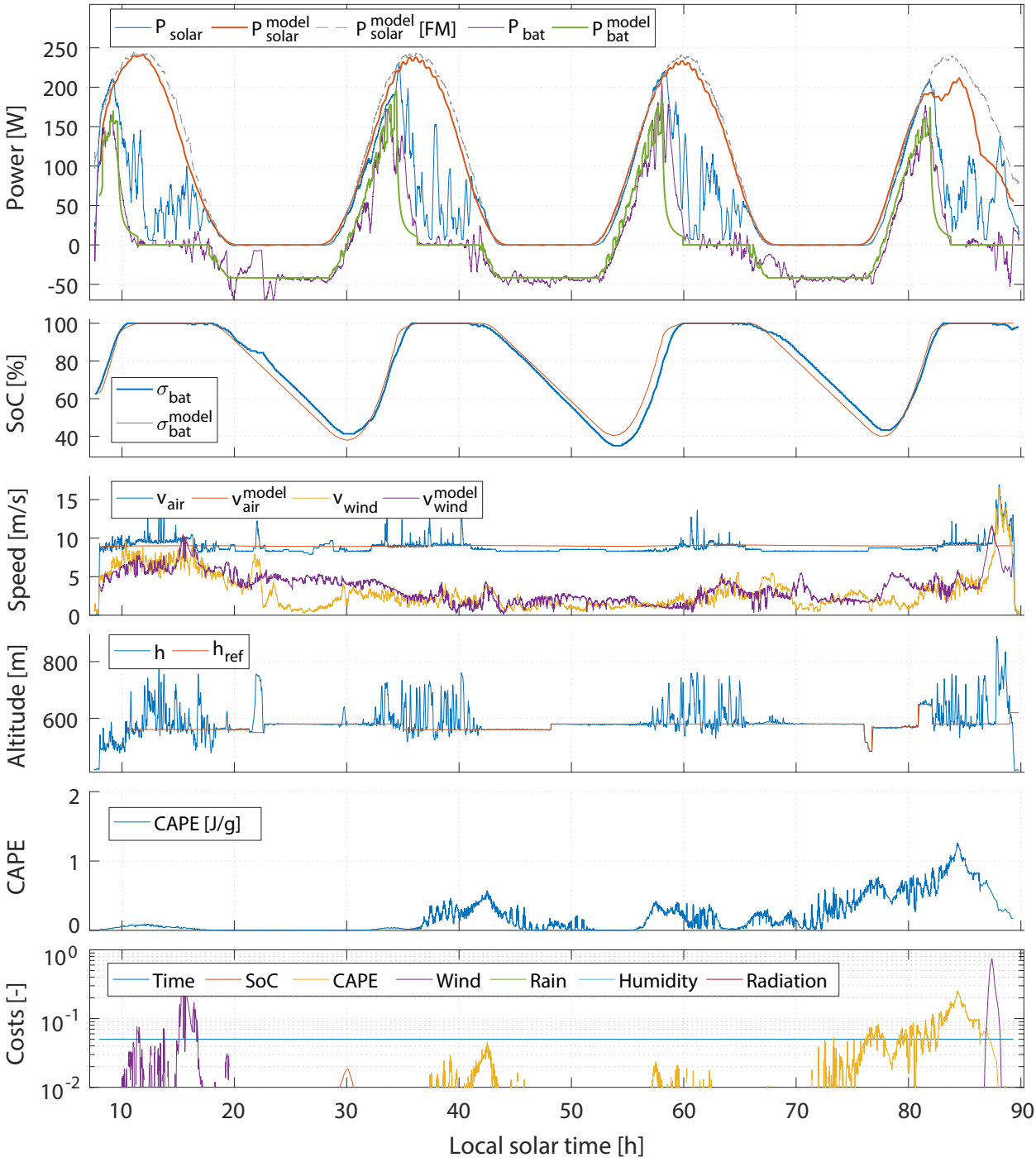

Fig. 13 Flight data from *AtlantikSolar*'s 81-hour continuous solar-powered loitering mission compared to the MetPASS planning results. The historical weather data used here correctly recovers the clear weather for days one to three and strong winds and thunderstorm clouds for the last day. The top plot shows solar power income P_{solar}(measured), $P_{\text{solar}}^{\text{model}}$(MetPASS), the clear-sky *full model* $P_{\text{solar}}^{\text{model}}$[FM] from [41], and battery power. The remaining plots show the state of charge, airspeed, wind conditions, the thunderstorm indicator CAPE and the individual MetPASS costs that especially the strong winds and high CAPE cause. Overall, the MetPASS predictions closely fit the flight data. Used with accurate weather data, MetPASS can thus predict and avoid unsafe situations such as the high winds close to thunderstorms on the last day.

approach their normalized limit ($\dot{C}_k = 1$). This correctly represents the significant danger the UAV is in. Unfortunately, these conditions were not predicted by the weather forecast from four days earlier. The main lesson learned is that positive initial weather reports together with the vast extent of data in modern weather models can quickly give a false sense of security to a user. Especially in multi-day missions the weather however changes so significantly that replanning *has* to be used, e.g. to avoid unsafe situations. In this case, the UAV could have simply been landed.

B. Point-to-Point Mission: Crossing the Atlantic Ocean

An Atlantic crossing, such as the 4000 km route from Newfoundland, Canada to Lisbon, Portugal, is an excellent demonstration case for long-endurance UAVs such as *AtlantikSolar*[‖]. Obviously, a thorough pre-assessment of the feasible flight conditions as well as continuous in-flight weather monitoring and route replanning are required.

Historical weather data: Determining optimal and marginal flight conditions Optimal and marginal border-cases and their performance metrics total cost, minimum SoC and flight time were identified using historical ECMWF weather data from 2012–2013. Figure 14 shows an optimal case: The route closely follows the orthodrome, with tailwind reducing the flight time to 52 h. Because the planner optimized the launch time, significant cloud cover can be avoided and $P_{\text{solar}} \approx P_{\text{solar}}^{\text{clear-sky}}$. Therefore, SoC> 17.2 %. The accumulated cost is $C = 2200$ and mainly consists of the time cost because all other components usually stay below their threshold. Marginal conditions are shown in Fig. 15. To avoid unsuitable areas (cross and headwind, humidity and low solar radiation), the planner chooses a path that deviates significantly from the orthodrome. The resulting flight time is 86 h. The minimum SoC is only 7.1 %. Although no cost reaches the critical limit β_k, the total accumulated cost is $C = 17800$. Launch is not recommended under these conditions. As described below, a more optimal nearby launch date can easily be determined using MetPASS.

Historical weather data: Determining the seasonal dependency of feasibility Due to the harsh Atlantic weather conditions it has to be assessed systematically when and how many launch windows exist. The performance metrics were thus assessed via MetPASS path optimizations performed in 6 h steps over the whole range from May 31st to August 8th for which historical ECMWF data was available. Figure 16 shows the minimum SoC and total accumulated cost. Even the first version of the *AtlantikSolar* UAV (AS-1 [42]) provides sufficient feasible launch dates from mid-May to end-July when requiring a SoC-margin of 10 %, and the later design revisions (AS-2 [10] and AS-3 [40]) would obviously only improve that performance. Additional analysis yields a minimum and average flight time of 52 h and 78 h respectively versus the 106 h for the no-wind unit test of Section III.B. Note that Fig. 16 can also be used before a flight to assess the quality of that launch date relative to all other launch dates of the season.

[‖] The Atlantic crossing inspired the name *AtlantikSolar* UAV. While technically feasible, the mission was not executed because of regulatory reasons, i.e. the fact that human-like sense-and-avoid capabilities were required by the aviation authorities but were not available.

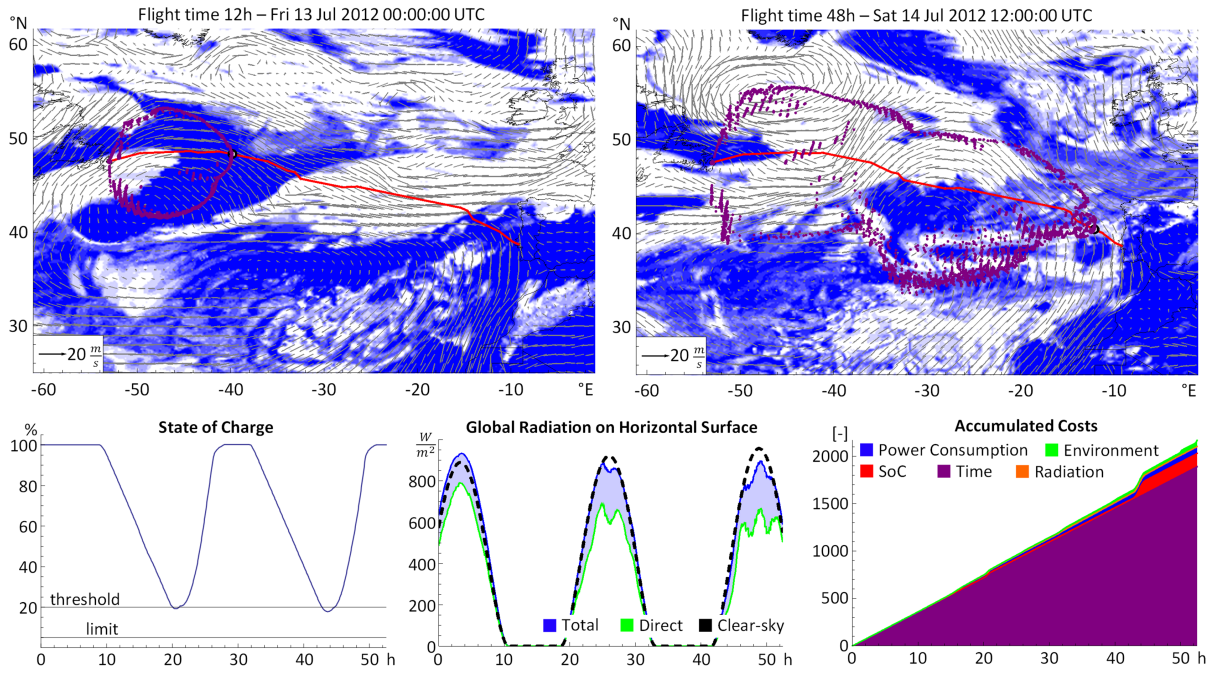

Fig. 14 A transatlantic flight in excellent conditions: MetPASS exploits the eastwards winds and retrieves an orthodrome-like path with only 52 h flight time. The SoC barely falls below the threshold. Except for the time cost, all costs are small. The Atlantic crossing is thus feasible if the launch time is chosen well.

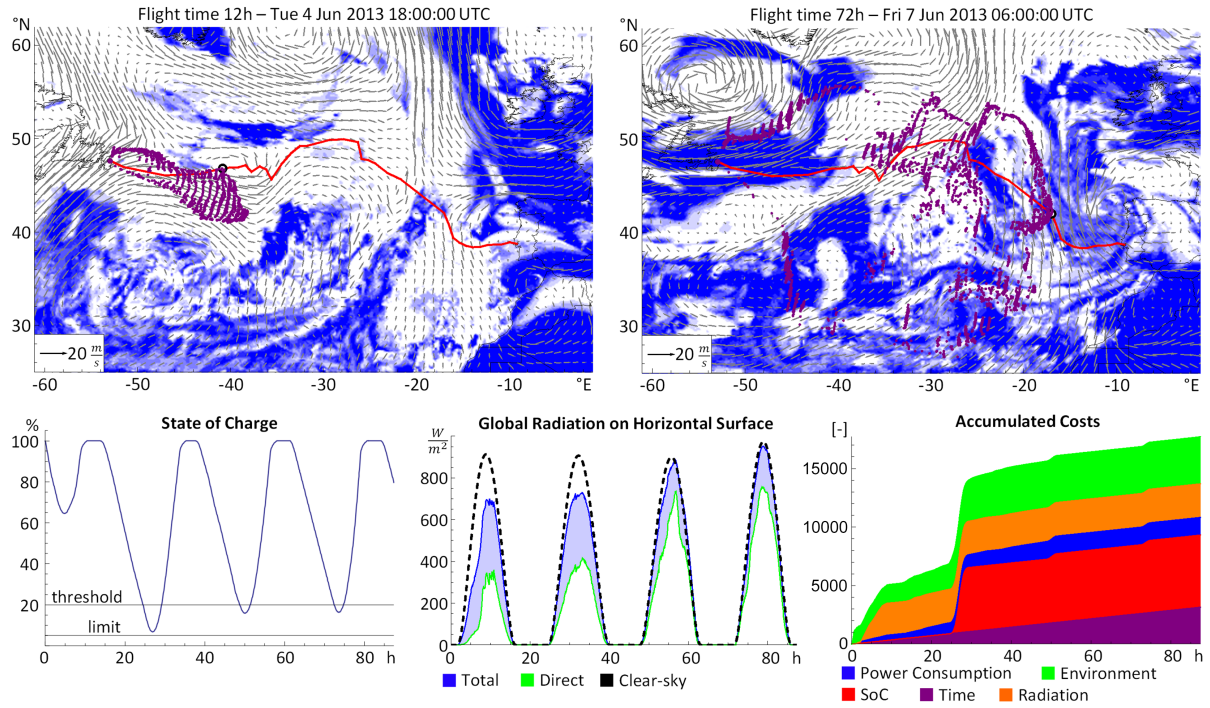

Fig. 15 A transatlantic flight in unsuitable conditions, i.e. unfavorable winds, cloud cover and thus critically-low SoC during the first night. The costs are a magnitude higher than for the excellent weather case. A feasible path is found, but the result clearly encourages to choose a different launch date using MetPASS.

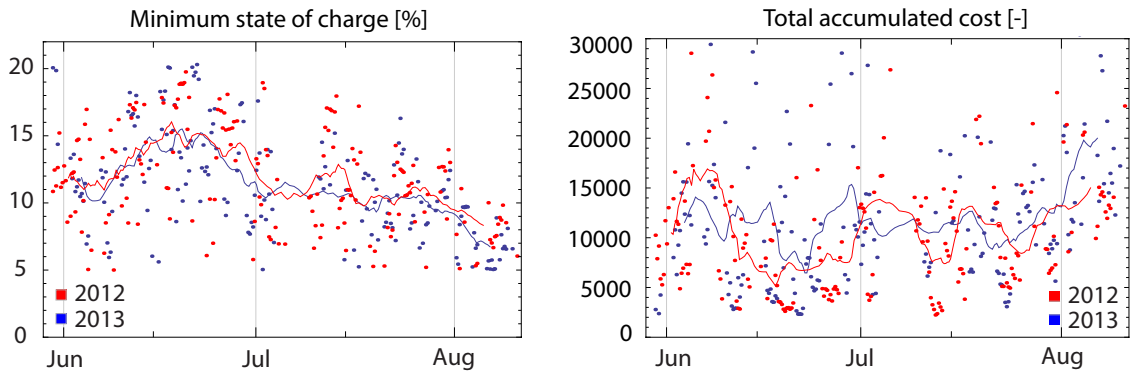

Fig. 16 Feasibility of an Atlantic crossing with *AtlantikSolar* AS-1 under historical ECMWF weather data from 2012–2013. Solid lines are the average of 20 surrounding days. Feasibility is highest around June 21st.

Forecasted weather data: Launch-time optimization and in-flight route replanning Figure 17 shows MetPASS' launch time optimization over a 50 hour window in April 2014. The subsequently used in-flight replanning capability allows to directly import and upload new waypoints to a UAV via common ground stations.

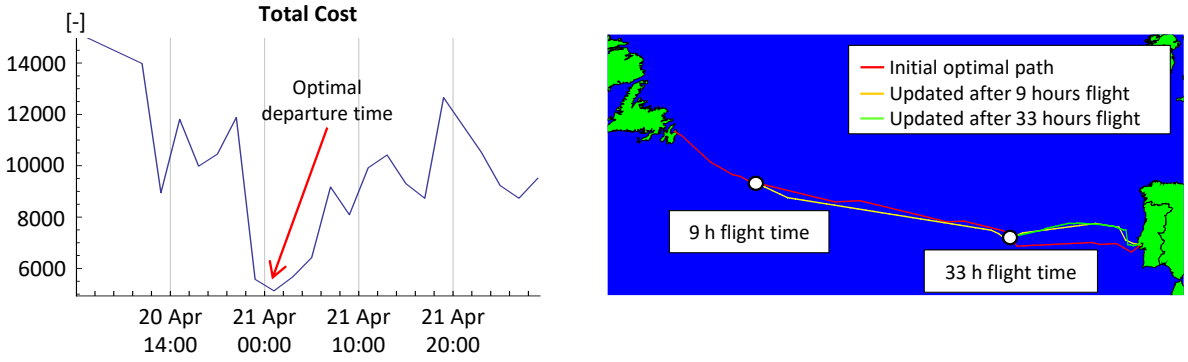

Fig. 17 MetPASS end-to-end planning process: Launch time optimization using weather forecasts from April 20th 2014 (left). Periodic in-flight replanning with updated weather data and waypoint retransmission (right).

C. Multi-Goal Missions: Inspecting Arctic Glaciers

Large-scale multi-goal missions optimally leverage solar aircraft. For example, the persistent aerial monitoring of Arctic glaciers and the analysis of their flow and calving characteristics is key to understanding climate change. Previously, glaciologists needed to use expensive transport (e.g. helicopters) to operate in remote places with limited infrastructure (tents without Internet) next to the glaciers [43]. The goal for *AtlantikSolar*'s 2017 Arctic deployment was thus to demonstrate a new paradigm: A complete scanning mission, i.e. take-off, inspection of one or more remote glaciers, and landing, from an easily-accessible home base (Qaanaaq, Greenland, Fig. 1). MetPASS performed both the feasibility assessment and the launch date and route optimization for the two missions presented below.

1. Two-Glacier Mission: Bowdoin Glacier

The inspection mission from Qaanaaq to Bowdoin glacier was performed on July 3rd 2017. Using forecasts from 15 h before takeoff, a clear-weather window was identified and take-off was performed at 16:26 local time (13.76h solar time). Two different scans were performed: One higher altitude lawn-mower scan at Bowdoin glacier, and one low-altitude stationkeeping scan at base. Figure 18 shows the path planned with the parameters of Table 2. The planner leverages the terrain avoidance ability that was extended over previous work [21]: Our simple method loads a Digital Elevation Model (in this case with 30 m horizontal resolution), applies horizontal terrain exaggeration to guarantee a certain distance to terrain and then calculates the *Altitude-AGL*-cost as described in Section II.A.2. Figure 18 also shows our automatic grid shifting approach: While by default the departure and arrival points are the center of the first and last grid slice (Fig. 3), which results in many grid points over inaccessible terrain, our grid shifting method maximizes the grid points over accessible areas such as the ocean. The optimized path is a time-optimal path that avoids terrain, i.e. *time* and *terrain* costs dominate. This is due to, first, the fjord-like terrain and maximum altitude restrictions which limit the path choices. Second, due to the small planning problem scale (compared e.g. to Section IV.B) the weather is rather homogeneous and exploiting these small weather differences is more expensive than a time-optimal path.

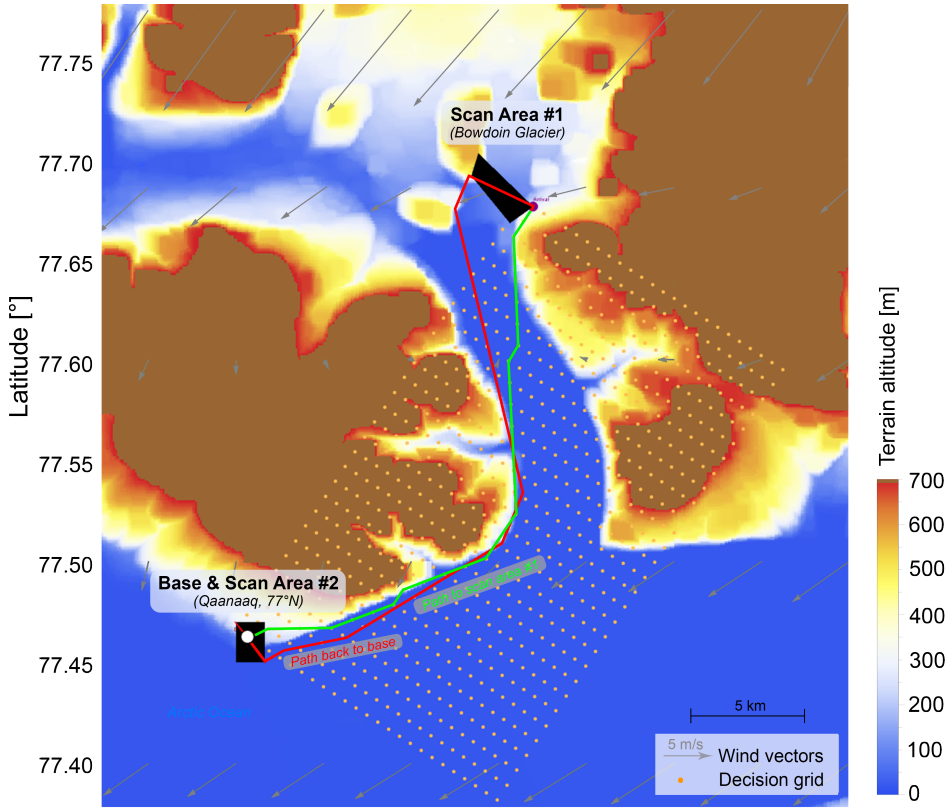

Fig. 18 ***AtlantikSolar*'s glacier inspection mission planned by MetPASS. The small problem scale and narrow fjords reduce the path choices. The path is a compromise between time-optimality and terrain-avoidance.**

Figure 19 compares *AtlantikSolar* flight data to the MetPASS predictions. The solar and battery power P_{solar} and

P_{bat} are again accurate. We only measure $P_{\text{solar}} < P_{\text{solar}}^{\text{model}}$ for $t = [13.8\,\text{h}, 15.6\,\text{h}]$ because $SoC \approx 100\,\%$ and P_{solar} is again throttled down by design. The battery discharge starts around 18.0 h solar time, where $P_{\text{bat}} < P_{\text{bat}}^{\text{model}}$ because of clouds. In contrast, the wind forecast is subject to significant errors: At $t \approx 16.8\,\text{h}$, the winds are $v_{\text{wind}} = 13.3\,\text{m/s}$ and $v_{\text{wind}}^{\text{model}} = 8.0\,\text{m/s}$ (at the northern scan path section at Bowdoin, Fig. 18). The measured and predicted time to complete each flight phase thus differ. More importantly, such wind speeds are a significant threat to the aircraft. While the high predicted winds were accounted for by flying at $v_{\text{air}} \approx 11\,\text{m/s} > v_{\text{air}}^{\text{opt}}$, MetPASS would have marked the flight as infeasible had the real wind speeds been known. Again, the strong winds would have been predicted by the forecasts available 3 h before launch. Overall, using MetPASS, this first-ever fully autonomous glacier inspection mission with a solar UAV in the Arctic could however be executed successfully. As predicted, the only significant cost or threat was the high wind speed at $t = [15.5\,\text{h}, 17.0\,\text{h}]$. The total flight duration was 4:52 h with 230 km distance, after which the batteries were still at SoC = 97 %. The whole mission was performed fully autonomously, i.e. without any pilot intervention. The scientific results provided to glaciologists were a full 3D reconstruction of Bowdoin glacier (Fig. 20) which showed a developing crack that led to a significant glacier calving event only days after the flight.

Planning-wise, two conclusions can be derived: First, the excellent weather makes this seem like a trivial mission that does not require a sophisticated planner. However, this was only because the planner had optimized the launch time and thus mission feasibility beforehand. The second lesson learned sounds trivial: Only up-to-date and more generally high quality weather data brings tangible benefits for mission planning. However, this has far-reaching implications: Not enforcing a weather data confidence check is a potential usage risk! In the long-term, probabilistic planning using ensemble weather forecasts [44] thus *needs* to be implemented to solve the issue in a mathematically sound way.

2. Six-Glacier Mission

MetPASS also planned an inspection mission to the six Arctic glaciers `A`–`F` in Fig. 1. The point-to-point grid was reduced to 12 slices and 9 vertices to reduce the calculation time (Table 2). The mission was not flown due to technical aircraft issues, but it neatly showcases the possibilities of solar-powered long-range flight in the Arctic. Figure 21 visualizes the 580 km and 16.3 h trajectory together with the aircraft position at 6:36 UTC and 17:00 UTC. The cloud cover and sun radiation situation is favorable, however, strong wind is indicated at the glaciers. The airspeed is thus increased from $v_{\text{air}}^{\text{opt}} = 8.6\,\text{m/s}$ to $v_{\text{air}} = 9.8\,\text{m/s}$ en route and $v_{\text{air}} = 11\,\text{m/s}$ inside the areas of interest. The path exploits the meso-scale winds which rotate counter-clockwise. In addition, when the straight-line path results in headwind, an alternate path (e.g. at t =6:36 UTC in Fig. 21 a path south of the straight line) is chosen. More importantly, the path avoids dangerous high-wind areas (except at t=11.2h after launch). The SoC stays above 68 % despite launch around solar midnight, thus confirming the potential of solar flight in summer in Arctic regions. Overall, the favorable weather and optimized path allow to avoid environmental risks and only result in *acceptable* costs that either increase flight safety (increased v_{air} and thus power consumption) or cannot be avoided (time and altitude AGL costs next to the glaciers).

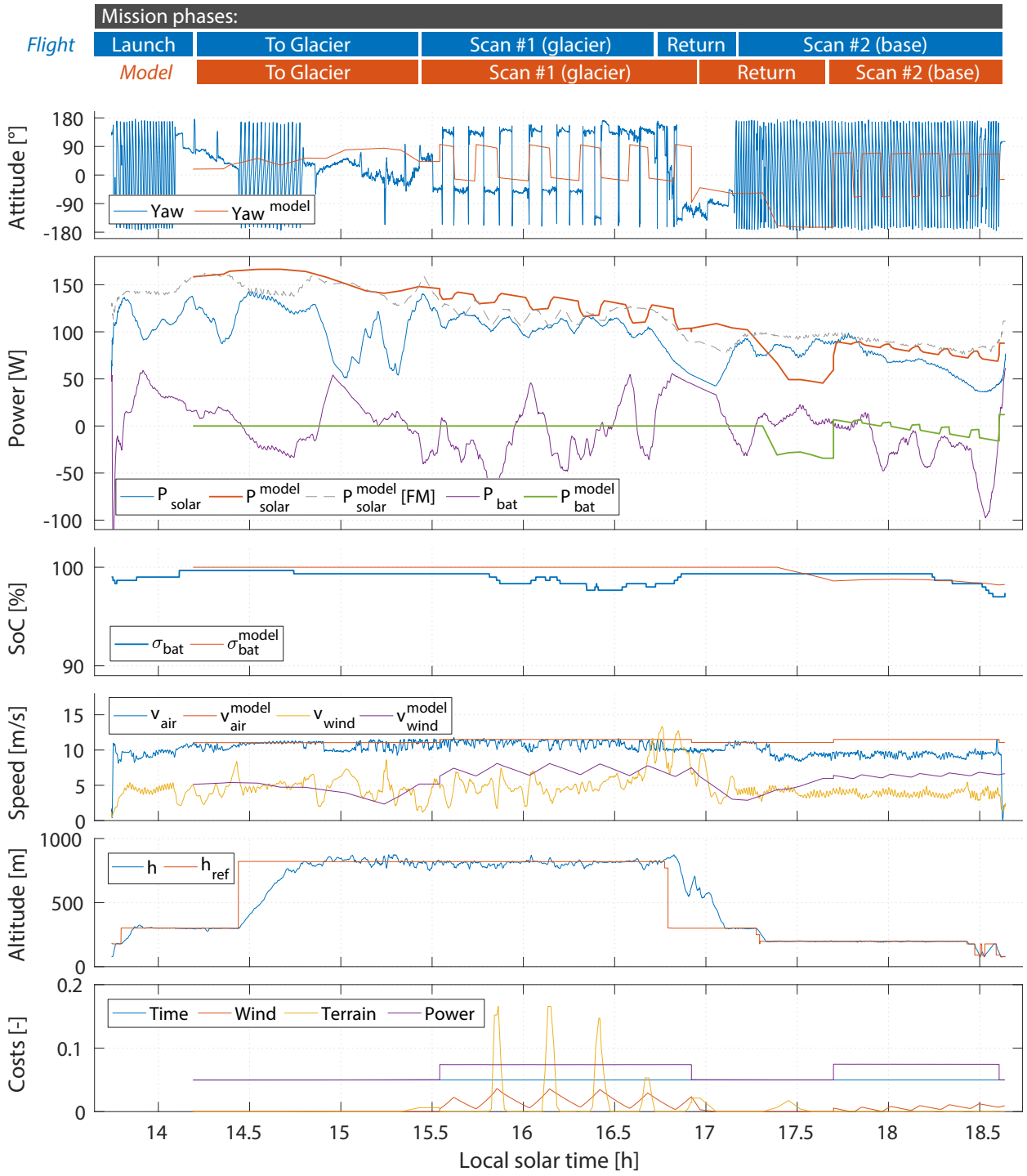

Fig. 19 The 4:52 h and 230 km glacier inspection mission performed by *AtlantikSolar* on July 3rd 2017 above the Arctic Ocean. The flight phases are indicated in blue for the flight data and in red for the MetPASS plan. They include start at the base in Qaanaaq, traveling to and scanning Bowdoin glacier and returning to base to perform a second aerial scan before landing. MetPASS used weather forecasts from 15 h before launch. The energy states are represented well, but erroneous wind forecasts cause significant differences in the time required to complete each flight phase. To preserve comparability, the MetPASS plan was therefore adapted to the same duration as the actual flight (only through shortening the second scanning phase a-posteriori).

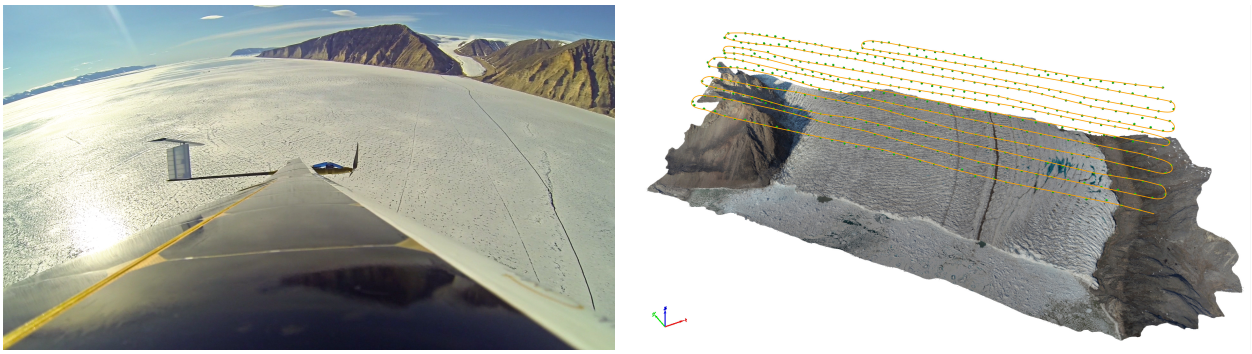

(a) (b)

Fig. 20 Left: The *AtlantikSolar* UAV operating over the Arctic sea ice next to Bowdoin glacier. Right: The 3D reconstruction (made with the commercial Pix4D software) of Bowdoin and the scan path. The scan area of 7 km^2 was covered with 75 % lateral overlap from 700 m AGL, which took 53 minutes and covered 47.7 km.

Table 3 compares the optimized path versus naive clockwise and counter-clockwise solutions. As expected, the MetPASS path is cost-optimal. The fact that it visits the nodes in the order `EF...` instead of `FE...` allows to avoid bad weather (in this case wind) and altitude AGL costs slightly better. However, the cost difference is < 1 % because the weather is favorable and no critical environmental risks (thunderstorms or precipitation) exist that would be avoided by MetPASS but not the naive path. The path distance is also similar, but compared to the clockwise path in which the aircraft flies against the global winds, the MetPASS flight time is 5 % lower. Note that in such good weather less trivial paths (those not strictly clockwise or counter-clockwise) always result in more flight time and thus cannot be optimal.

Table 3 The path optimized by MetPASS against the naive solutions.

	MetPASS	Clockwise	Counter-clockwise
Cost	5595	5634 (+0.7 %)	5650 (+1.0 %)
Time	16.3 h	17.1 h (+4.9 %)	16.2 h (-0.6 %)
Distance	580 km	579 km (-0.2 %)	572 km (-1.4 %)
Order	EFDCBA	ABCDEF	FEDCBA

D. Computational Performance Analysis

The computation time plays a significant role especially for in-flight re-planning. As shown in Table 4, first, even multi-day stationkeeping missions (81h-flight) are calculated within seconds as they do not require route planning but only straightforward system state propagation. Second, large-scale point-to-point missions (4000 km Atlantic crossing) require point-to-point route optimization, which takes below 10 minutes. Third, multi-goal inspection missions require the scan path optimization, heuristics calculation and an inter-goal optimization that includes either $n_{\text{heuristic}}$ or n_{naive} point-to-point route optimizations depending on whether the heuristic is used. The two-glacier mission is optimized in 11 minutes. The heuristic is not advantageous because it a) takes longer to calculate than all point-to-point optimizations

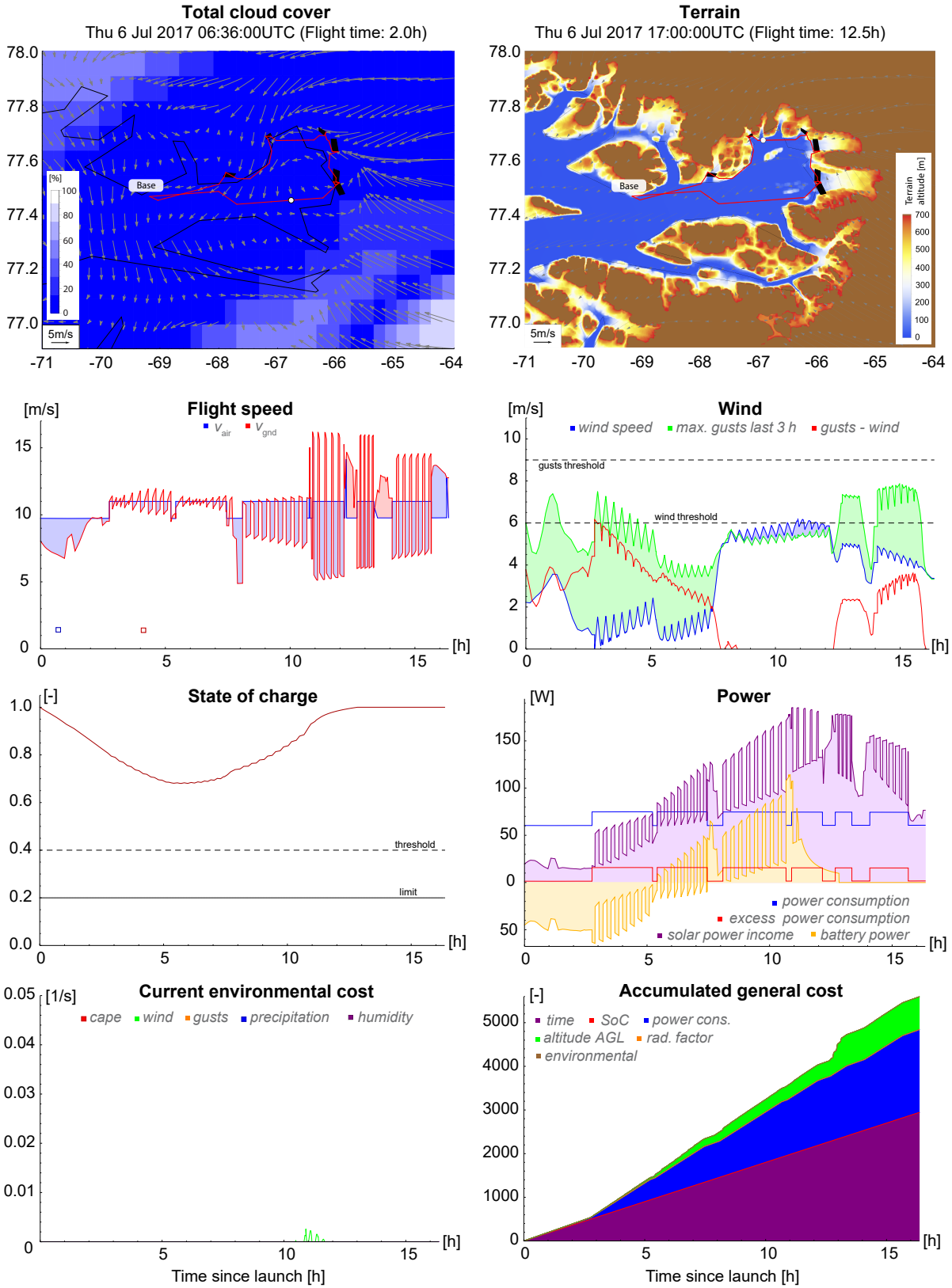

Fig. 21 The six-glacier scan mission in the Arctic. The MetPASS path is shown against cloud cover (top left) and terrain (top right). The weather conditions are favorable: The environmental costs are close to zero and the main costs are excess power consumption (due to winds), altitude above ground and time. Despite strong winds the SoC never dips below 68 %, indicating the potential of solar flight in Arctic regions.

Table 4 Computation times with a 2.8 GHz quad-core Intel Xeon E3-1505M CPU with 16GB RAM and the parameters of Table 2. The total computation time t_{total} consists of the scan path and heuristic computation times $t_{\text{scanpaths}}$ and $t_{\text{heuristic}}$ and the route optimization time t_{opt} (which includes the inter-goal and point-to-point optimization). The six-glacier mission benefits significantly from using the heuristic.

Mission	**81h-Flight**	**Atlantic**	**Arctic** Two glaciers	**Arctic** Six glaciers
t_{total}, of which	16 s	462 s	690 s	1010 s
$\cdot\, t_{\text{scanpaths}}$	-	-	1 s	3 s
$\cdot\, t_{\text{heuristic}}$	-	-	579 s	538 s
$\cdot\, t_{\text{opt}}$	16 s	462 s	110 s	469 s
$n_{\text{heuristic}}$	-	-	6	161
n_{naive}	-	-	6	2676
$n_{\text{heuristic}}/n_{\text{naive}}$	-	-	1.0	0.06

and b) does not reduce the number of edge cost evaluations. In contrast, for the six-glacier mission, the 9 minutes to calculate the heuristic allow to reduce the required edge cost calculations by 94 %. The calculation time t_{total} with heuristic is 17 minutes** and is thus, based on a simple extrapolation, 8 times less than if all edge costs were calculated.

Figure 22a analyzes the heuristic quality between vertices v and w , i.e. $q_{\text{heuristic}} = \frac{h_{vw}}{c_{vw}} = \frac{\text{heuristic value}}{\text{actual cost}}$. Here, $q_{\text{heuristic}} \leq 1$ must hold for a valid heuristic, but the closer $q_{\text{heuristic}}$ gets to unity the earlier suboptimal paths can be sorted out. The $q_{\text{heuristic}}$ achieved in this work was analyzed by calculating h_{vw} and c_{vw} for 600 point-to-point problems: The departure time (and thus weather) was chosen randomly in a 3-day window. The departure and arrival coordinates were chosen randomly across Europe but within 10–50 km of each other. Overall, the mean heuristic quality is only 20 %. Recall however that we define the heuristic as the orthodrome path cost under the best weather conditions in the whole planning area and time interval. Often, a tiny good-weather spot in otherwise bad weather exists such that h_{vw} is small but c_{vw} is large. Figure 22b evaluates the influence of $q_{\text{heuristic}}$ on the number of edge cost evaluations. At large N, the heuristic is significantly more effective at reducing the required edge cost calculations. While the number of edge cost evaluations is heavily dependent on the problem statement and the weather data, especially large problems can be sped up if future research improves the heuristic. For example, for $N = 7$ improving $q_{\text{heuristic}}$ to 70 % allows an order-of-magnitude reduction in edge cost computations. Even today, MetPASS however already calculates large-scale stationkeeping, point-to-point and multi-goal missions at sufficient grid resolution in below 20 minutes (Table 4).

V. Conclusion

This paper presented MetPASS, the Meteorology-aware Trajectory Planning and Analysis Software for Solar-powered UAVs. Using dynamic programming and an A*-algorithm with a custom heuristic, optimal paths for large-scale stationkeeping, point-to-point and multi-goal inspection missions are generated. MetPASS is the literature's first

**Note however that, compared to the two-glacier mission, the grid resolution was reduced in return for a fast computation.

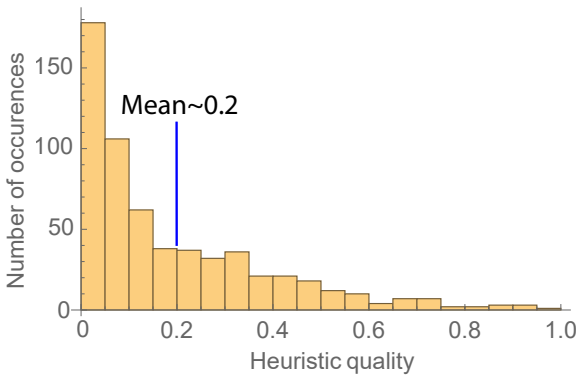

(a) The heuristic quality distribution computed in 600 experiments with random boundary conditions (start time, departure and arrival coordinates). The mean heuristic quality is 20 %.

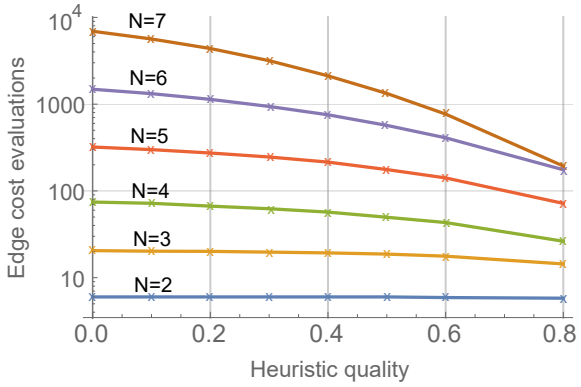

(b) The number of required edge cost evaluations as a function of heuristic quality and areas of interest N. Each data point was obtained by simulating 10 randomly generated problems.

Fig. 22 Heuristic quality and the resulting performance gains.

framework that considers *all* aspects that affect solar flight safety and performance: It avoids environmental risks (thunderstorms, rain, gusts) and exploits advantageous regions (clear sky or tailwind) using historical or forecasted weather data, avoids system risks (e.g. low battery) through a system model, and navigates through cluttered terrain. The resulting point-to-point paths are cost-optimal while the multi-goal paths are cost-optimal for small scan area size.

Three different missions are presented to analyze the planner and to show what is possible with today's solar UAVs: *AtlantikSolar*'s 2338 km and 81 h endurance world record flight, a hypothetical 4000 km Atlantic crossing, and a 230 km two-glacier and 580 km six-glacier remote sensing mission above the Arctic Ocean. Most of these missions could be executed successfully — and in favorable weather — due to the fact that MetPASS performed the launch time optimization. In unstable weather, as visible in the Atlantic Crossing feasibility analysis, MetPASS' mathematically structured approach to combining an aircraft system model with meteorological data becomes even more important to reliably and efficiently perform large-scale solar aircraft missions. For example, while the no-wind flight time for the Atlantic crossing is 106 h, the correct selection of launch date and flight path via MetPASS yields only 52 h flight time.

Overall, the fact that large-scale solar-powered missions with small UAVs are still exceptionally hard to perform means that a statistically-significant quantitative analysis of MetPASS' planning quality and benefits is still pending. Nevertheless, the amount of experimental data in this paper is unparalleled in the current solar aircraft or planning literature and allows to derive further qualitative lessons learned:

- *Cost advantages to naive solutions:* The cost advantages generated by incorporating weather data *significantly* decrease with, first, less weather variability (as in good macro weather situations) because less areas with above-average weather conditions can be exploited, second, small planning areas that also implicitly decrease weather variability, and third, high or cluttered terrain that limits the valid path choices.
- *Quality of weather data:* The extent of data available from today's meteorological models can give a false sense

of planning security. Tangible planning benefits are however only possible if properly maintained high-quality data is used. For example, for the Arctic missions, the go or no-go decision using the $t_{\text{launch}} - 15\,\text{h}$ and $t_{\text{launch}} - 3\,\text{h}$ weather data was entirely different, and the 81-hour flight showed that in-flight replanning is equally key. Future mission planning frameworks including MetPASS should thus enforce a weather data confidence check before planning. In the long term, probabilistic planning using ensemble weather forecasts [44] should be implemented (e.g. via stochastic dynamic programming [23]) to automatically take care of forecast uncertainty.

Acknowledgements

This research was partially funded by the Sun2Ice project under ETH Grant ETH-12 16-2 with funds of the Dr. Alfred and Flora Spälti and ETH Zurich Foundation. It was also supported by a number of generous individuals and project partners[††].

References

[1] Colella, N., and Wenneker, G., "Pathfinder: Developing a solar rechargeable aircraft," *IEEE Potentials*, Vol. 15, No. 1, 1996, pp. 18–23.

[2] Weider, A., Levy, H., Regev, I., Ankri, L., Goldenberg, T., Ehrlich, Y., Vladimirsky, A., Yosef, Z., and Cohen, M., "SunSailor: Solar powered UAV," Tech. rep., Aerospace Engineering Faculty, Technion, 2007. http://webee.technion.ac.il/people/maxcohen/SunSailorArt19nov06.pdf.

[3] Malaver, A. J. R., Gonzalez, L. F., Motta, N., and Villa, T. F., "Design and Flight Testing of an Integrated Solar Powered UAV and WSN for Remote Gas Sensing," *IEEE Aerospace Conference*, 2015.

[4] AeroVironment, "AeroVironment Solar-Powered Puma AE Small Unmanned Aircraft Achieves Continuous Flight for More Than Nine Hours," Press release, August 12th 2013. http://www.avinc.com/resources/press_release/aerovironment-solar-powered-puma-ae-small-unmanned-aircraft-achieves-contin.

[5] ByeAerospace, "Industry First: Solar-Electric Silent Falcon Prepares for Initial Customer Orders," Press release, March 15th 2015. http://www.byeaerospace.com/news/2016/3/2/industry-first-solar-electric-silent-falcon-prepares-for-initial-customer-orders.

[6] Cocconi, A., "AC Propulsion's solar electric powered SoLong UAV," Tech. rep., AC Propulsion, 2005. Retrieved from https://archive.org/details/ACPropulsionSolongUAV2005.

[7] Noth, A., "Design of Solar Powered Airplanes for Continuous Flight," Ph.D. thesis, ETH Zurich, 2008.

[8] British Broadcasting Corporation (BBC), "Solar Impulse lands in California after Pacific Crossing," , Apr. 2016. http://www.bbc.com/news/science-environment-36122618. Retrieved 10/12/2017.

[††] A list of project partners is available at http://www.atlantiksolar.ethz.ch/?page_id=187

[9] QinetiQ, "QinetiQ files for three world records for its Zephyr Solar powered UAV," Press release, August 24th 2010. https://www.aero-mag.com/qinetiq-files-for-three-world-records/.

[10] Oettershagen, P., Melzer, A., Mantel, T., Rudin, K., Stastny, T., Wawrzacz, B., Hinzmann, T., Leutenegger, S., Alexis, K., and Siegwart, R., "Design of Small Hand-Launched Solar-Powered UAVs: From Concept Study to a Multi-Day World Endurance Record Flight," *Journal of Field Robotics (JFR)*, Vol. 34, No. 7, 2017, pp. 1352–1377. doi:10.1002/rob.21717.

[11] Sridhar, B., Ng, H. K., and Chen, N. Y., "Aircraft trajectory optimization and contrails avoidance in the presence of winds," *Journal of Guidance, Control and Dynamics*, Vol. 34, No. 5, 2011, pp. 1577–1583.

[12] Rubio, J. C., and Kragelund, S., "The trans-pacific crossing: Long range adaptive path planning for UAVs through variable wind fields," *Digital Avionics Systems Conference, 2003. DASC'03. The 22nd*, Vol. 2, IEEE, 2003, pp. 8–B.

[13] Rubio, J. C., Vagners, J., and Rysdyk, R., "Adaptive path planning for autonomous UAV oceanic search missions," *AIAA 1st Intelligent Systems Technical Conference*, 2004, pp. 20–22.

[14] Chakrabarty, A., and Langelaan, J., "Flight Path Planning for UAV Atmospheric Energy Harvesting Using Heuristic Search," *AIAA Guidance, Navigation and Control Conference*, 2010.

[15] Chakrabarty, A., and Langelaan, J., "UAV Flight Path Planning in Time Varying Complex Wind-Fields," *American Control Conference (ACC)*, 2013.

[16] Klesh, A., and Kabamba, P., "Energy-optimal path planning for solar-powered aircraft in level flight," *AIAA Guidance, Navigation and Control Conference and Exhibit*, American Institute of Aeronautics and Astronautics, 2007.

[17] Klesh, A. T., and Kabamba, P. T., "Solar-Powered Aircraft: Energy-Optimal Path Planning and Perpetual Endurance," *Journal of Guidance, Control, and Dynamics*, Vol. 32, 2009.

[18] Spangelo, S., Gilbert, E., Klesh, A., Kabamba, P., and Girard, A., "Periodic energy-optimal path planning for solar-powered aircraft," *AIAA Guidance, Navigation, and Control Conference*, 2009. doi:10.2514/6.2009-6016.

[19] Hosseini, S., Dai, R., and Mesbahi, M., "Optimal Path Planning and Power Allocation for a Long Endurance Solar-Powered UAV," *American Control Conference (ACC), 2013*, IEEE, 2013, pp. 2588–2593.

[20] Dai, R., "Path Planning of Solar-Powered Unmanned Aerial Vehicles at Low Altitude," *Circuits and Systems (MWSCAS), 2013 IEEE 56th International Midwest Symposium on*, IEEE, 2013, pp. 693–696.

[21] Wirth, L., Oettershagen, P., Ambuehl, J., and Siegwart, R., "Meteorological Path Planning Using Dynamic Programming for a Solar-Powered UAV," *IEEE Aerospace Conference*, 2015. doi:10.1109/AERO.2015.7119284.

[22] Bellman, R., "On a routing problem," *Quarterly of applied mathematics*, Vol. 16, No. 1, 1958, pp. 87–90.

[23] Bellman, R., *Dynamic Programming*, Courier Corporation, 2013. First published by Princeton University Press, Princeton, New Jersey, 1957.

[24] Ambühl, J., "Sailing the virtual Bol d'Or," Scientific Report MeteoSwiss 98, MeteoSwiss, 1998. P. 44. http://www.meteoswiss.admin.ch/home/services-and-publications/publications.html.

[25] Wirth, L., "Meteorological path planning using Dynamic Programming for a solar-powered Atlantic-crossing Unmanned Aerial Vehicle," Master's thesis, ETH Zurich, 2014.

[26] Cornwall, C., "Solar Equations Document," Tech. rep., Earth System Research Laboratory, 2014. https://www.esrl.noaa.gov/gmd/grad/solcalc/solareqns.PDF.

[27] Fischer, H. S., and Gilgen, H., "DACHRad - Berechnung der direkten Sonneneinstrahlung in Deutschland, Österreich und der Schweiz," Bulletin of the Geobotanical Institute, ETH Zurich, 2002.

[28] Pamadi, B. N., *Performance, Stability, Dynamics, and Control of Airplanes*, 2nd ed., AIAA Education Series, 2004.

[29] Hoffman, K. L., Padberg, M., and Rinaldi, G., *Traveling Salesman Problem*, Springer US, Boston, MA, 2013, pp. 1573–1578. doi:10.1007/978-1-4419-1153-7_1068.

[30] Bellman, R., "Dynamic Programming Treatment of the Travelling Salesman Problem," *Journal of the ACM (JACM)*, Vol. 9, No. 1, 1962, pp. 61–63. doi:10.1145/321105.321111.

[31] Malandraki, C., and Daskin, M. S., "Time Dependent Vehicle Routing Problems: Formulations, Properties and Heuristic Algorithms," *Transportation Science*, Vol. 26, No. 3, 1992, pp. 185–200. doi:10.1287/trsc.26.3.185.

[32] Malandraki, C., and Dial, R. B., "A restricted dynamic programming heuristic algorithm for the time dependent traveling salesman problem," *European Journal of Operational Research*, Vol. 90, No. 94, 1996, pp. 45–55. doi:10.1016/0377-2217(94)00299-1.

[33] Schneider, J., "The time-dependent traveling salesman problem," *Physica A: Statistical Mechanics and its Applications*, Vol. 314, No. 1-4, 2002, pp. 151–155. doi:10.1016/S0378-4371(02)01078-6.

[34] Testa, L. J., Esterline, A. C., Dozier, G. V., and Homaifar, A., "A Comparison of Operators for Solving Time Dependent Traveling Salesman Problems Using Genetic Algorithms," *Proceedings of the 2nd Annual Conference on Genetic and Evolutionary Computation*, 2000.

[35] Bertsekas, D. P., *Dynamic Programming and Optimal Control, Volume 1*, 3rd ed., Athena Scientific, Belmont, MA, 1995.

[36] Hart, P. E., Nilsson, N. J., and Raphael, B., "A Formal Basis for the Heuristic Determination of Minimum Cost Paths," *IEEE Transactions on Systems Science and Cybernetics*, Vol. 4, No. 2, 1968, pp. 100–107.

[37] Hamacher, H. W., Ruzika, S., and Tjandra, S. A., "Algorithms for time-dependent bicriteria shortest path problems," *Discrete Optimization*, Vol. 3, No. 3, 2006, pp. 238–254. doi:10.1016/j.disopt.2006.05.006.

[38] Chabini, I., and Lan, S., "Adaptations of the A* Algorithm for the Computation of Fastest Paths in Deterministic Discrete-Time Dynamic Networks," *IEEE Transactions on Intelligent Transportation Systems*, Vol. 3, No. 1, 2002, pp. 60–74. doi:10.1109/6979.994796.

[39] Förster, J., "Multi-Goal Meteorological Path Planning for a Solar-Powered Unmanned Aerial Vehicle," Semester thesis, ETH Zurich, 2017.

[40] Oettershagen, P., Stastny, T., Hinzmann, T., Rudin, K., Mantel, T., Melzer, A., Wawrzacz, B., Hitz, G., and Siegwart, R., "Robotic Technologies for Solar-Powered UAVs: Fully-Autonomous Updraft-Aware Aerial Sensing for Multi-Day Search-and-Rescue Missions," *Journal of Field Robotics (JFR)*, 2018. doi:10.1002/rob.21765.

[41] Oettershagen, P., and Siegwart, R., "High-Fidelity Solar Power Income Modeling for Solar-Electric Aircraft: Development and Flight Test Based Verification," *33rd European PV Solar Energy Conference and Exhibition (PVSEC)*, 2017. doi: 10.4229/EUPVSEC20172017-6BV.2.46.

[42] Oettershagen, P., Melzer, A., Mantel, T., Rudin, K., Lotz, R., Siebenmann, D., Leutenegger, S., Alexis, K., and Siegwart, R., "A Solar-Powered Hand-Launchable UAV for Low-Altitude Multi-Day Continuous Flight," *IEEE International Conference on Robotics and Automation (ICRA)*, 2015. doi:10.1109/ICRA.2015.7139756.

[43] Jouvet, G., Weidmann, Y., Seguinot, J., Funk, M., Abe, T., Sakakibara, D., Seddik, H., and Sugiyama, S., "Initiation of a major calving event on the Bowdoin Glacier captured by UAV photogrammetry," *The Cryosphere*, Vol. 11, No. 2, 2017, pp. 911–921. doi:10.5194/tc-11-911-2017.

[44] Molteni, F., Buizza, R., Palmer, T. N., and Petroliagis, T., "The ECMWF Ensemble Prediction System: Methodology and Validation," *Quarterly Journal of the Royal Meteorological Society*, Vol. 122, No. 529, 1996, pp. 73–119.